The Pennsylvania State University

The Graduate School

Department of Civil and Environmental Engineering

SIMPLIFIED NUMERICAL BRIDGE MODEL SUBJECT TO BLAST LOADS

A Thesis in

Civil Engineering

by

Corinne Seifert

Submitted in Partial Fulfillment
of the Requirements
for the Degree of

Master of Science

August 2014

The thesis of Corinne M. Seifert was reviewed and approved* by the following:

Jeffrey A. Laman
Professor of Civil Engineering
Thesis Advisor

Daniel G. Linzell
Professor of Civil Engineering

Peggy A. Johnson
Professor of Civil Engineering
Head of the Department of Civil and Environmental Engineering

*Signatures are on file in the Graduate School

ABSTRACT

Damage to a pier column will take a bridge out-of-service, or worse, lead to a complete bridge failure. Besides the importance of civilian safety, maintaining bridge serviceability is imperative to civilian and military transport, while discontinuous transportation networks have rippling effects on economy and community. With the increase of blast attacks on transportation networks and structures, researchers and design engineers are seeking understanding of the behavior of transportation structures subject to blast loading.

Increased numerical modeling capabilities allow researchers to consider material, structural, and load effects on structure response at limited expense. However, researchers must carefully consider modeling parameters to appropriately represent the nonlinear material and geometric behavior inherent to a blast event. Numerical model simulations vary vastly in complexity and are handicapped by programming assumptions. A balance of numerical model fidelity, simulation behavior accuracy and general applicability must be found to develop design criterion for blast loads on bridge components.

This study considers the effects of four modeling parameters: aspect ratio, boundary conditions, longitudinal reinforcement ratio and standoff distance in a simplified and a complex numerical simulation. The simplified model considers several discrete mass elements connected by linear elements to model the subject column, whereas the complex model considers continuum elements, material models accounting for degradation and failure, and a built-in blast load application software. The scope of the project was to evaluate the performance of the simplified model considering the

complex model as the baseline for comparison. It is believed that the differences in load application, material behavior, and stiffness have the largest impact on the simplified model. Implementation of the load application and stiffness must be carefully considered in the development of a simplified model.

TABLE OF CONTENTS

LIST OF FIGURES

LIST OF TABLES

ACKNOWLEDGEMENTS

I would like to thank my committee, Dr. Jeffrey Laman, Dr. Daniel Linzell, and Dr. Andrew Scanlon for their advice during the completion of this thesis. Also, I would like to thank John Lobo for his input in developing the simplified model. And finally, I would like to thank the Department of Civil and Environmental Engineering and my family for their support.

Chapter 1

Introduction

1.1 Background

Recent events have increased the demand to design and retrofit structures to resist blast loads. Much of the published research and guidelines on blast resistant design is related to buildings and public safety, however, bridge engineers also must consider the risks associated with short duration, high intensity, blast loads.

Recommendations for Bridge and Tunnel Security (FHWA, 2003) offers suggestions to improve security and reduce bridge and tunnel vulnerability. Security features for signature bridges, such as the Brooklyn Bridge or the Golden Gate Bridge are in place; however, these features are not implemented for many of the most critical transportation links. These links must be protected against blast load to ensure a safe and reliable transportation network.

Currently, the American Association of State Highway and Transportation Officials (AASHTO) *LRFD Bridge Design Specifications* contain no specific guidelines for the analysis and design of bridges to resist blast loading. Other specifications, such as the U.S. Department of Defense's Unified Facilities Criteria (UFC) 3-340-02 *Structures to Resist the Effects of Accidental Explosions* presents methods of design for facilities but has no bridge-specific information.

Supporting pier columns are considered one of the most critical and vulnerable parts of a bridge (NCHRP, 2010). If a column collapses, multiple spans or the entire

structure may collapse. An increasing number of engineers are beginning to consider the structural integrity of bridges in response to blast loading because of the importance of bridge pier columns with respect to maintaining structural integrity.

1.2 Problem Statement

There is a need for specification development for analysis and design of bridges under blast loading. This study will focus on the analysis of bridge columns subjected to blast loads, which is important to the development of a comprehensive specification.

There are many methods available to engineers to predict blast loads and the response of bridge components. However, there are no guidelines or design specifications from AASHTO or FHWA for simplified analyses that can be used efficiently in conjunction with a blast design process. Sophisticated models are not practical because they involve large computational requirements, costly software, and time commitments that are not available to the practicing engineer. In addition, detailed models are not always warranted because of high uncertainties associated with the size and location of the explosive (NCHRP Report 645). As a result, a need exists to develop and validate efficient bridge-specific simplified modeling techniques that provide economical and accurate results.

1.3 Objectives

This study will investigate the accuracy of simplified models in efforts to develop new design guidelines and specifications. The objective of this study is to evaluate the effectiveness of a proposed simplified model of bridge columns under blast loading. The

accuracy and limitations of the simplified modeling technique are examined by comparing shear, moment, and deformation magnitudes over the time-history of a blast event for the columns studied to validated, advanced, finite element analysis (FEA) results.

1.4 Scope

This study investigates the effects of blast loading on round, concrete bridge columns by comparing the results of high-level, detailed, dynamic, finite element analyses (FEA) using LS-DYNA to a proposed, simplified numerical simulation technique using SAP2000. The simplified numerical simulation is a multi-degree of freedom (MDOF), uncoupled analysis composed of linear elements and discrete masses that represent the column mass and the superstructure mass analyzed in SAP2000. The LS-DYNA finite element model, composed of solid and beam elements, features a MDOF coupled approach involving an explicit, dynamic, time-history analysis.

A parametric study using LS-DYNA and SAP2000 was completed to investigate the performance of the simplified modeling technique and possible limitations as compared to the LS-DYNA models. CONWEP was used to generate the blast loads used in the LS-DYNA and SAP2000 models.

All of the columns considered in this study have the following parameters:

- A diameter of 1524 mm (60 in);
- Concrete compressive strength of 27.57 MPa (4000 psi);
- Grade 60 reinforcement;
- Concrete cover of 76.2 mm (3 in);
- Column axial load of $0.12(f'_c A_g)$;

- Transverse reinforcement ratio equal to the maximum of $\rho_s \geq 0.45\left(\frac{A_g}{A_c} - 1\right)\frac{f'_c}{f_y}$ and $\rho_s \geq 0.18\frac{f'_c}{f_y}$;
- Charge weight of 226.8 kg (500 lb) TNT;
- A column height of 7620 mm (25 ft) or 16,764 mm (55 ft);
- A longitudinal reinforcement ratio of 1% or 2%;
- A standoff distance of 1.22 m (4.0 ft) or 7.62 m (25.0 ft);
- Boundary conditions of a free cantilever, propped cantilever, or construction joint at the base of the column.

1.5 Task List

The following tasks were completed to accomplish the objectives of this study:

1. Literature Review

   A literature review was completed to determine the current state of practice related to simplified modeling of bridge columns with blast loading. Blast loading origins and available blast analysis methods were also examined. Modeling techniques, assumptions, parameters, and material models were investigated to help with the decisions for the LS-DYNA and SAP2000 models for this study.

2. Computational Modeling

   Simplified numerical simulations of blast loading on bridge columns were conducted in SAP 2000 based on a previously established procedure (John Lobo, personal communication, Jan. 2012) that simplifies the blast loading and analyses. The simplified numerical simulation developed by Lobo was explored in this study; and analyses were completed based on this method. Detailed finite element models were created with LS-DYNA with blast loads generated using CONWEP, which is an empirically-based blast load function.

3. Parametric Study

   Varied parameters include: 1) aspect ratio; 2) longitudinal reinforcement ratio; 3) boundary conditions; and 4) scaled distance.

4. Computational Results and Comparison

   Data from the SAP2000 and LS-DYNA models were compared to determine the effectiveness of the simplified model. Output data that were compared include deflected shape, moment envelopes, and shear envelopes.

5. Conclusions and Recommendations

   After the results from the LS-DYNA and SAP2000 models were compared, limitations of the simplified model were outlined. Recommendations on how to make the simplified model more accurate are provided in terms of load determination and analysis method. Recommendations on how to implement simplified analysis of bridge pier columns under blast loading into design specifications are also provided.

Chapter 2

Literature Review

This literature review focuses on blast loading, blast analysis methods, as it relates to modeling techniques, assumptions, parameters, and material models. The current state of practice related to simplified numerical simulation of bridge piers subjected to blast loading is also presented. Relevant results and findings on these topics that support decisions related to creating, examining, and comparing finite element and simplified numerical simulation used to complete the study are presented.

2.1 Blast Loading

Accurate modeling of bridge substructure blast response, irrespective of the modeling technique used, is dependent on the accuracy of the loads that represent the blast. Therefore, general blast loading information, along with commonly accepted methods used to represent pressure time-histories, is summarized and computer programs commonly used to develop blast propagation information are discussed.

Load distributions and durations caused by a conventional air blast are often defined as a function of the charge weight, W, and the standoff distance, R (T. Ngo et al., 2007). Air blast loads are also affected by the shape of the explosives and their orientation relative to the structure (Baylot et al., 2003).

During a blast event, an incident pressure wave travels from the center of the charge toward the target as presented in Figure 2-1. At the arrival time, t_A, pressure suddenly increases to a peak overpressure, P_{S0}, relative to the ambient pressure. The

pressure then decays to the ambient level at time t_A+t_d. The pressure further decays to a negative pressure, creating a partial vacuum, beyond t_A+t_d.

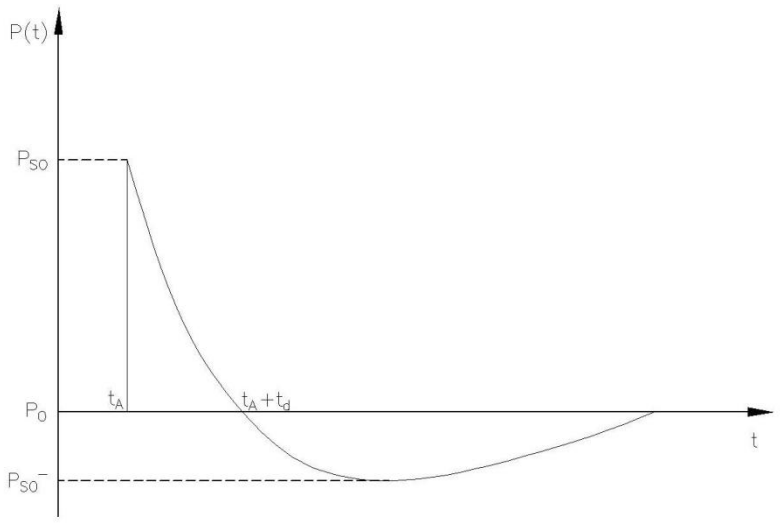

Figure 2-1: Blast Wave Pressure-Time History (Ngo et al., 2007)

The incident peak overpressure is amplified when the shock wave is reflected off an object in its path. In addition, pressure builds up in confined areas until the reflected waves are vented (Winget et al., 2005). When modeling bridge pier columns, it is important to account for the reflected waves by accurately representing the surrounding environment. Waves may reflect off the ground surface or the superstructure (Williamson et al., 2010). As a result, the ground surface needs to be addressed when modeling bridge piers because those reflected pressures reach the base of the column first and may create additional reflected waves that could add more loading to the column (Williamson et al., 2010). Pressures at the top of the column are lower and arrive much later than at the bottom (Williamson et al., 2010) and, as a result, confinement of waves

due to the superstructure will likely not control the response of the bridge pier columns. Therefore, only the ground surface needs to be modeled.

Bridge columns are subjected to large lateral forces from explosions below the deck. The lateral forces may cause large deformations, shear, or flexural failure (Winget et al., 2005). Cratering and spalling of a concrete column may cause a loss of cover, especially if there is a small standoff distance that could result in failure of the column. Under blast loading, spalling is defined as a tensile failure caused by a shock wave traveling through the column and reflecting off the back face, reversing direction, and creating tension forces as it travels back to the center of the member. Cratering is defined as compression failure on the blast face (Winget et al., 2005).

2.1.1 Blast Wave Propagation Programs

Shock-wave propagation programs use computational fluid dynamics to predict the pressure time-histories on a structure. The most widely used blast wave calculation program is BlastX (SAIC, 1994). Although BlastX is the most common program, it is limited to U.S. Government agencies and is not available to the general public. Another commonly applied tool that helps to develop an empirically-based, blast load function is the CONWEP code that is integrated into a commonly used advanced finite element program, LS-DYNA (LSTC, 2014).

CONWEP calculates blast loads on a structure for a TNT weight at a given standoff distance. It uses empirical blast models developed by Kingery and Bulmash (Randers-Pierson and Bannister, 1997) and produces a pressure load in terms of a

reflected pressure, incident pressure, and angle of incidence (Sriram et al., 2006) as shown in Equation (2-1):

$$P=P_1\cos^2\theta+P_2(1-\cos\theta)^2 \quad (2\text{-}1)$$

where: P_1 = reflected pressure; P_2 = incident pressure; and θ = angle of incidence.

CONWEP uses the Hopkinson-Cranz (Hopkinson 1915, Cranz 1926) cubic root scaling law to calculate loads on the structure for a given TNT weight at a given distance (LSTC, 2014). The scaling law states that a peak pressure will occur at a distance from the explosion that is proportional to the cube root of the energy yield as shown in Equation (2-2):

$$Z=\frac{R}{W^{1/3}} \quad (2\text{-}2)$$

where: R = distance from the center of the explosion; W = weight of standard explosive; and Z = scaled distance.

Using Equation (2-2), similar blast waves are produced for the same scaled distances when two explosive charges of different weights are detonated in the same atmospheric conditions. CONWEP is valid for scaled distances between 0.054 and 39.7 $m/kg^{1/3}$ (0.136 and 100 $ft/lbm^{1/3}$).

2.2 Blast Analysis Methods

In addition to determining accurate loads, an appropriate analysis numerical simulation must be employed when modeling blast loads on bridge pier columns. Different analysis methods are available to engineers examining blast loading structural response. When used for bridge pier column design and retrofit, the method that is

employed should be efficient and give accurate results. Blast analysis methods that are commonly available have been grouped into the following general categories (Winget et al., 2005): uncoupled vs. coupled; static vs. dynamic; and single-degree-of-freedom (SDOF) vs. multi-degree-of-freedom (MDOF).

There are advantages and disadvantages to each method. An uncoupled analysis calculates the loads and structural response separately. While an uncoupled analysis is easy to perform, it overestimates the loads because member yielding and failure, which reduce the structure's stiffness and lead to increased deflections, are not taken into account (Winget et al., 2005). A coupled analysis takes into account the effects of the structural response on the behavior of the blast load and, thereby, provides more accurate results. Ultimate behavior is better predicted using a coupled analysis, but large computational times are required.

A static analysis calculates a single force in time from the time-pressure variations of the blast load. This type of analysis only accounts for one deformation mode. Inertial forces are not included. Inaccurate results are common in static analyses because it is difficult to accurately calculate the single, one-time force (Winget et al., 2005). Unlike a static analysis, a dynamic analysis takes into account inertial effects and provides more accurate results.

A SDOF analysis is the current state of practice with respect to analyses used to assist with the blast design of bridge pier columns (Williamson et al, 2010). While using a more complex analysis method could provide more accurate results, a detailed analysis is not justified with the unpredictability of the size and location of the charge. A SDOF analysis provides reasonably accurate results for simple structures, but it is difficult to

correctly model complex structures (Winget et al., 2005). However, a SDOF analysis allows for a large number of load cases and structural configurations to be modeled because of the simplicity of the calculations. A MDOF analysis accounts for more modes in the response of the system and provides accurate results for complex structures but requires more computational time when compared to a SDOF analysis (Winget et al., 2005).

A linear or nonlinear analysis can be performed using many analysis programs. There are two types of nonlinearity: material behavior and large displacements. A bilinear stress-strain response or a more accurate, nonlinear, representation of material properties can be used to model material stress-strain nonlinearity. Geometric nonlinearity, which refers to changes in load and stiffness as the structure deforms, should be modeled to account for phenomena such as moment magnification from P-Δ effects (Winget et al., 2005).

The most common blast analysis method is a SDOF or MDOF, uncoupled, dynamic analysis (Winget et al., 2005). Loads are calculated using a shock-wave propagation program such as BlastX or CONWEP. Both of these programs account for reflected waves, confinement effects, and pressure magnification (Williamson et al., 2010). Pressure-time histories from the shock-wave propagation program are then applied to the structure and the structure is analyzed. Two analyses are performed, one that calculates the loads on the structure and a second that determines the response of the structure. As a result, the load calculations are not coupled to the structural response. Therefore, a coupled analysis may be required if the surroundings change significantly during the loading period. Coupled analyses are not typically performed because of the

amount of computer resources required, but a coupled analysis results in a more accurate prediction of structural response.

2.3 Model Assumptions, Parameters, and Materials

This section summarizes research related to finite element and simplified modeling of blast loaded, reinforced concrete, bridge pier columns. Included in this discussion are commonly used modeling assumptions and examined parameters. Research on widely accepted concrete material models under blast load is also summarized along with LS-DYNA material models that have been shown to be accurate for analyzing reinforced concrete blast load situations.

LS-DYNA will be used in this study because of its proven effectiveness for modeling structures under blast loads (LSTC, 2014; NCHRP, 2010). CONWEP is incorporated into LS-DYNA as a blast load generation function and, as a result, loads can be readily applied to the models.

2.3.1 Model Assumptions

A common approximation accepted when bridge pier blast analysis research has been conducted is neglecting superstructure live and dead loads. This is a conservative approximation if flexural failure is assumed to govern behavior (Winget et al., 2005). For reinforced concrete columns, an increase in flexural capacity can result from increasing the axial load until the balanced point of failure is reached, the point at which the maximum compression strain is reached on one face of the column simultaneous with tensile yield strain in the layer of reinforcement farthest from the compression face. Figure 2-2 presents the balanced point on a representative pier column axial-moment

interaction diagram. This approximation of neglecting superstructure live and dead loads is not conservative if there is a high axial load, where the failure point is above the balanced point on the interaction diagram because there is not an increase in flexural capacity if the axial load is included.

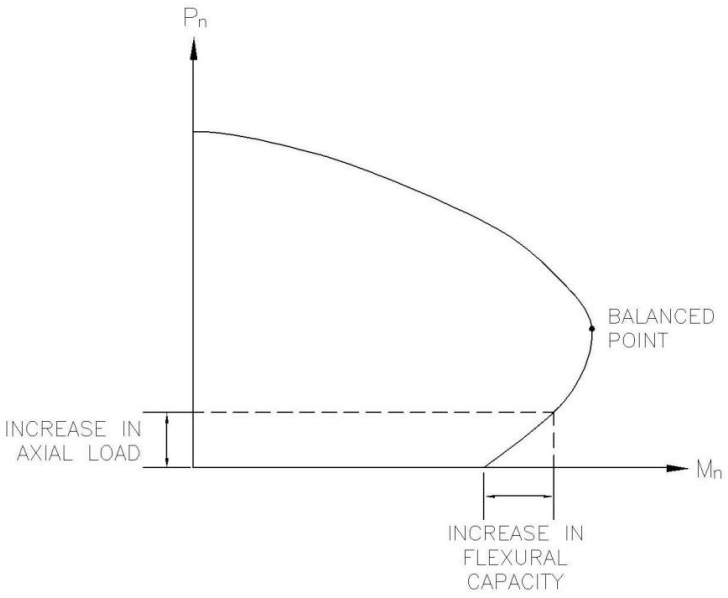

Figure 2-2 Representative Interaction Diagram

The ground surface around the bridge column must be included in the model to allow for reflection of blast waves off the ground (Winget et al., 2005). Reflected waves create additional loading on the structure and more accurately replicate actual conditions. The ground can be modeled as infinitely rigid to account for reflection of the waves (O'Hare, 2011).

A propped cantilever support condition is a common modeling assumption for pier columns. It is recognized that a below-deck explosion causes uplift forces sufficient to overcome the gravity loads on the girders and if the girders are connected to the columns, a net tensile force may result on the columns. However, girder uplift forces are

assumed to be negligible due to simple bearing pad support conditions that are commonly used (Winget et al., 2005). This results in a propped cantilever support condition that prevents longitudinal translation in a direction parallel to the bridge axis.

2.3.2 Parameters

There are many types of bridges and structural systems in use. This results in an extensive variety with respect to the design of bridge pier columns. As a result, it is important to statistically analyze the population to focus the research on representative, or characteristic, columns therefore offering representative and broadly useful results. These characteristic columns can then be modeled to include a wide range of design possibilities.

In the study by Williamson et al. (NCHRP, 2010), ten, half-scale, representative columns were physically tested under blast loads. The representative columns had varying cross-sections and sizes, longitudinal reinforcement ratios, reinforcement splice locations, and transverse reinforcement types and spacing. The parameters that were used are presented in Table 2-1. These parameters were selected based on a survey of several state DOTs design and detailing standards. According to Williamson, three cross-sections are common in bridge column design: circular, rectangular, and oblong. Circular columns are most economical and the most commonly constructed based on the survey. Rectangular columns are also regularly constructed; therefore square columns were included in the study by Williamson. Column sizes were based on minimum column dimension specifications from state DOTs. Splice locations of the longitudinal reinforcement were based on the location of the inflection point as a result of the assumed

boundary conditions. The type of transverse reinforcement varies from state to state, but most DOTs prefer discrete hoops. Spiral reinforcement has increased confinement compared to hoops, so spiral reinforcement was also included in the study by Williamson. The volumetric reinforcement ratio depends on the governing loading condition.

Table 2-1 Column Parameter Summary (Williamson et al., 2010)

	Column Geometry		Long. Reinf.	Transverse Reinf.		
Column Test No.	Shape	Size, cm (in.)	Splice Location	Pitch/Space, cm, (in.)	Type	Vol. Ratio ρ_s %
1	Round	45.72 (18)	0.25L	15.24 (6.0)	Hoops	0.82
2	Round	45.72 (18)	0.25L	15.24 (6.0)	Hoops	0.82
3	Round	45.72 (18)	0.25L	15.24 (6.0)	Spiral	0.82
4	Round	76.2 (30)	0.25L	15.24 (6.0)	Hoops	0.47
5	Round	76.2 (30)	0.25L	15.24 (6.0)	Hoops	0.47
6	Round	76.2 (30)	none	15.24 (6.0)	Spiral	0.47
7	Round	76.2 (30)	none	8.89 (3.5)	Spiral	0.80
8	Round	76.2 (30)	0.25L	5.08 (2.0)	Spiral	1.40
9	Square	76.2 (30)	0.25L	15.24 (6.0)	Ties	0.47
10	Square	76.2 (30)	0.25L	5.08 (2.0)	Ties	1.40

2.3.3 Material Models

LS-DYNA contains many material models that represent both concrete and reinforcement steel under blast loads. Magallanes (2008) studied concrete material models in LS-DYNA under blast and impulse loads. Several concrete constitutive models were compared by examining their ability to reproduce laboratory observations and predict response of structures subjected to blast loading. It was concluded that only material models using an Equation of State (EOS) approach to represent the tri-axial stress states correctly modeled the response of concrete flexural members under blast

loading. An EOS is a constitutive equation that determines the hydrostatic behavior of a material by calculating pressure as a function of volume and internal energy. LS-DYNA material types 72, 72 release 3, and 159 were shown to produce reliable results for concrete under blast loads when compared to lab tri-axial and blast test observations (Magallanes, 2008).

Material type 72 is a modified version of material type 16 (LSTC, 2014). Material type 16 uses an equation of state to give the current pressure as a function of current and previous minimum (most compressive) volumetric strain. Volumetric and deviatoric components of stress have different effects on material behavior. Due to the decoupling of volumetric and deviatoric responses, this model does not incorporate shear dilation of concrete under load (Malvar et al., 1997). Material type 72 has three shear failure surfaces to represent yield, maximum, and residual strengths which are shown in Figure 2-3. During loading, the deviatoric stresses remain elastic until reaching the yield surface, shown as point 1 in Figure 2-3. The stresses can increase until the maximum yield surface is reached, which is shown as point 2 in Figure 2-3. Beyond this point, the response is perfectly plastic.

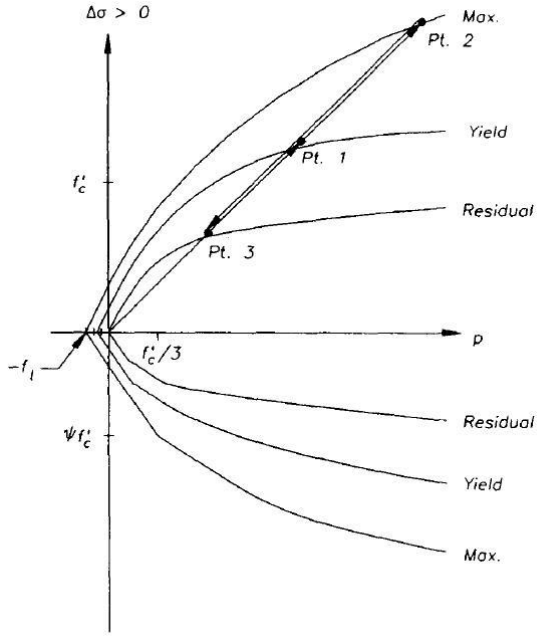

Figure 2-3 DYNA Material Type 72 Failure Surfaces (Malvar et al., 1997)

Material type 72 release 3 is the latest revision of Material Type 72. Material type 72 release 3 was developed by Karagozian & Case, Inc. and has the same three-shear failure surfaces as material type 72 (LSTC, 2014). The most significant user improvement to release 3 is the model parameter generation capability based on the 28 day compressive strength of the concrete (LSTC, 2014). This modification allows for default parameters to be defined for normal weight concrete and requires minimal user input.

Material type 159 is a smooth or continuous cap model available exclusively for solid elements, which limits its application when compared to the previously discussed LS-DYNA material types. This material model has a smooth intersection between the shear yield surface and hardening cap, which is shown in Figure 2-4. The user can input material properties or use default material properties for normal strength concrete (LSTC, 2014). Material type 159 uses a three-invariant yield surface like material type 72 and a

return algorithm for plasticity. Damage accumulation is based on brittle and ductile damage. Ductile damage accumulates when the damage threshold is exceeded and the pressure is compressive. Brittle damage accumulates with the damage threshold is exceeded and the pressure is tensile. A softening function applies a damage parameter equal to the maximum of the brittle or ductile damage parameters to the six elemental stress components. Strain rate effects are modeled using viscoplasticity.

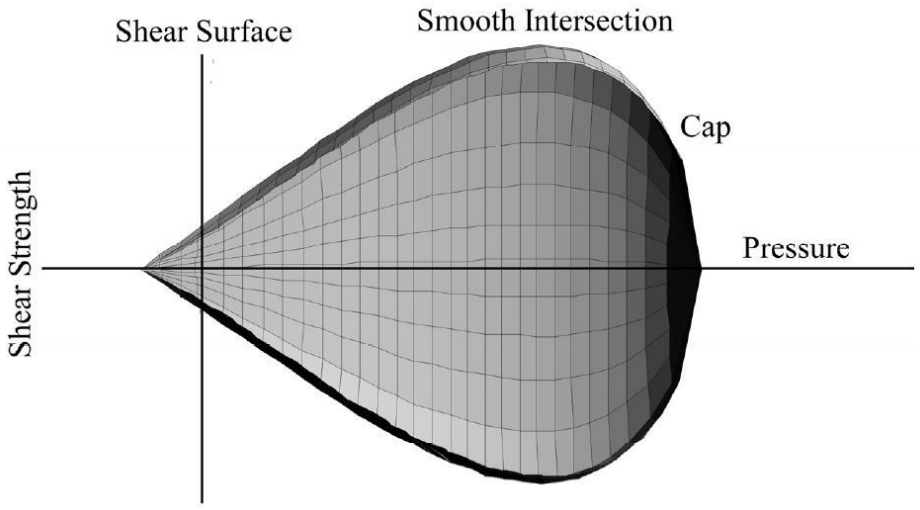

Figure 2-4 LS-DYNA Material Type 159 Yield Surface (LSTC, 2014)

Material Type 159 was used in this research to model the concrete based on work by O'Hare (2011), which showed that blast loaded bridge pier columns were accurately modeled using this material model when compared to experimental results.

When examining the behavior of reinforced concrete components under blast loads, material type 3 had been reported as being good for modeling the reinforcing steel. Material type 3 is a bilinear elasto-plastic model and can be used with either kinematic or isotropic strain hardening (LSTC, 2014). The center of the yield surface is fixed in

isotropic strain hardening, but its radius is a function of the plastic strain. For kinematic hardening, the center of the yield surface is fixed but can translate in the direction of the plastic strain. The strain rate is accounted for using the Cowper and Symonds model, which scales the yield stress with the factor $1+\left(\frac{\dot{\epsilon}}{C}\right)^{1/\rho}$, where $\dot{\epsilon}$ is strain rate, and C and ρ are strain rate hardening coefficients.

High strain rates affect the behavior of the reinforcing steel. Reinforcing bars can experience a yield stress increase of 60 percent or more, depending on the grade of steel (Malvar, 1998). Material type 24 can account for the increase in capacity caused by high strain rates in the reinforcing steel. Material type 24 is an elasto-plastic model with an arbitrary stress vs. strain curve and an arbitrary strain rate dependency that can be defined (LSTC, 2014). Strain rate effects can be defined in three different options. In the first option, the strain rate can be accounted for using the Cowper and Symonds model. The second option is to input a load curve to scale the yield stress. The third option is to input a table with different stress vs. strain curves for different strain rates (LSTC, 2014). Material type 3 was used in the present study to model the steel reinforcement based on work by O'Hare (2011), which showed that blast loaded bridge pier columns were accurately modeled using this material model for the steel reinforcement when compared to experimental results.

2.4 Finite Elements

The concrete material models require the use of three-dimensional solid brick elements. As a result, the LS-DYNA models created for the present study utilize constant stress solid elements to model the concrete. Previous research (FHWA, 2011; O'Hare,

2011) has reported that constant stress solid elements produce accurate results for blast loaded concrete while requiring significantly less computational time when compared to fully integrated solid elements.

Beam elements were used to represent both the vertical reinforcement and ties. Two beam elements are available in LS-DYNA for this application: the Hughes-Liu and the Belytschko-Schwer elements (LSTC, 2014). O'Hare (2011) reported that both elements have been shown to perform well and selected the Hughes-Liu beam element because the Hughes-Liu beam element is incrementally objective, which means that rigid body rotations do not generate strains, and the element allows for the treatment of finite strains. These issues are important to determine second order effects in the element. In addition, the Hughes-Liu beam element is compatible with solid elements that will be used to model the concrete because the Hughes-Liu formulation is based on a degenerated brick element formulation (LSTC, 2014). In contrast to the Hughes-Liu element, the Belytschko-Schwer beam element uses a co-rotation technique in the element formulation for treating large rotations. A co-rotation technique separates the deformation and rigid body deformations by using two coordinate systems: 1) element coordinates that are coordinates that deform with the element; and 2) body coordinates that rigidly rotate with the nodes. The current orientation of the element coordinates is compared to the initial coordinate system to determine deformations. No numerical integration is performed over the cross-section in the Belytschko-Schwer beam element, therefore it is slightly more computationally efficient when compared to the Hughes-Liu element. However, the Belytschko-Schwer beam element may be less accurate because there is no numerical integration over the cross-section and, as such, assumes constant

stress across the cross-section (LSTC, 2014). Due to the accuracy of the Hughes-Liu beam element and the compatibility with the solid elements, the Hughes-Liu element was selected to model the steel reinforcement in the present study.

2.5 Simplified Models

A simplified numerical simulation incorporates many approximations in an attempt to efficiently and conservatively yet accurately model blast loads on bridge pier columns and the structural response. The current guidelines for the simplified blast analysis of bridge pier columns are summarized in this section.

The National Cooperative Highway Research Program (NCHRP) Report 654, *Blast-Resistant Highway Bridges: Design and Detailing Guidelines* (2010), provides guidelines for a simplified blast analysis of a bridge pier column. It states that a SDOF analysis is warranted due to high uncertainty related to the explosion definition. For a SDOF analysis the plastic moment capacity, the total mass of the member, and the moment of inertia need to be determined. Design material strengths used in the calculation of the plastic moment capacity need to be increased to account for actual material strengths and strain rate effects. The time-history, magnitude, and distribution of the blast load also need to be estimated using available load prediction methods. These methods include charts in the U.S. Army's TM 5-1300 *Structures to Resist the Effects of Accidental Explosions* (1990), which has been superseded by Unified Facilities Criteria (UFC) 3-340-02, *Structures to Resist the Effects of Accidental Explosions* (2008), or information from software such as CONWEP and BlastX. A representative blast loading chart from UFC 3-340-02 is presented in Figure 2-5. The chart can be used to

determine peak positive incident pressure, P_{so}, and peak positive normal reflected pressure, P_r, based on a scaled distance, Z.

The resulting load should be distributed and vary with time and must approximate a load that varies with position. This equivalent load should be used to complete a plastic analysis of the column where its effect and the equivalent mass and stiffness of the structural system should be determined to transform the actual structure into a representative SDOF or MDOF system. An example of the SDOF system for a column is shown in Figure 2-6. Once the equivalent SDOF system is developed, the maximum deflections and maximum support rotations can be calculated and used to determine if the column can withstand the blast load.

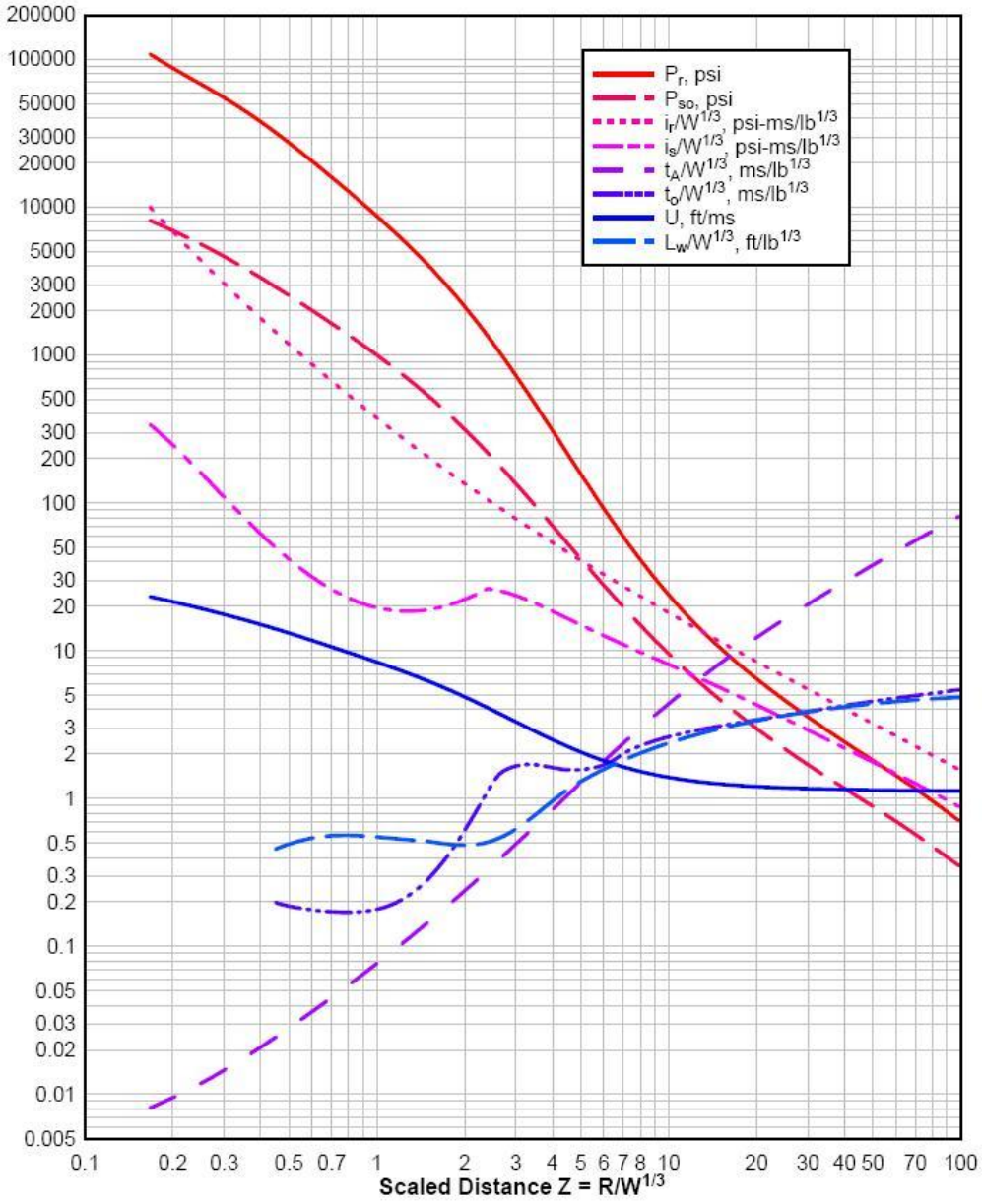

Figure 2-5 Positive Shock Wave Parameters for a Hemispherical TNT Explosion on the Surface at Sea Level (UFC 3-340-02, 2008)

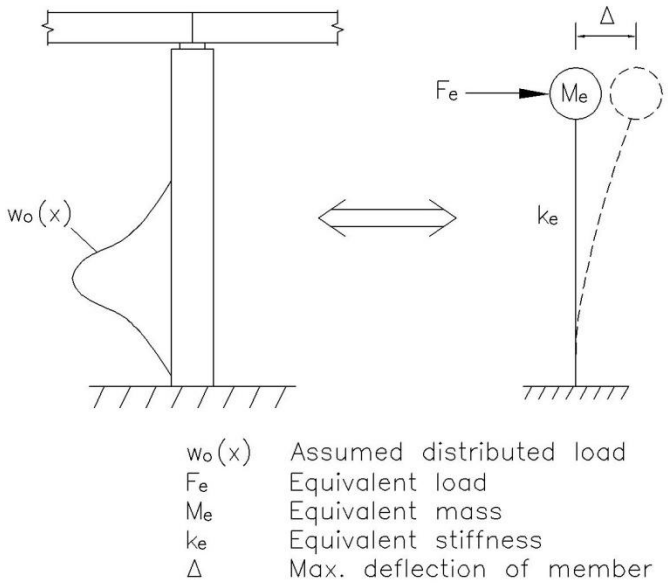

Figure 2-6 Relationship between real system and equivalent SDOF system

If a MDOF model was used for the structure in Figure 2-6, it would appear as detailed in Figure 2-7. A MDOF system would differ from SDOF discussed above by including more modes of the response by using lumped masses with a load applied to each lumped mass. The simplified method that is being evaluated in this study will follow the MDOF because, as discussed earlier, MDOF analyses provide more accurate results when compared than SDOF analyses (Winget et al., 2005).

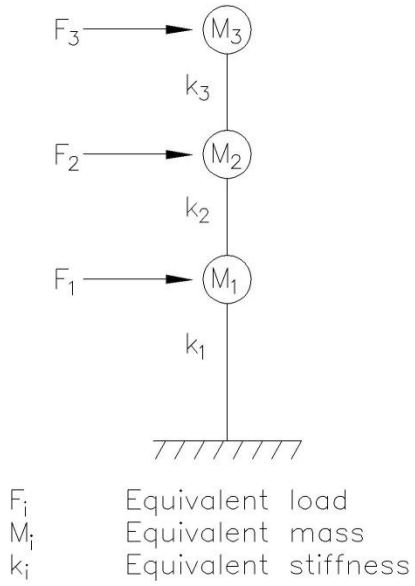

Figure 2-7 Equivalent MDOF System

2.6 Summary

Literature reviewed in this chapter was used to make modeling decisions for the current research and included a summary of the current state of practice for modeling blast loads on bridge columns. General blast loading and blast wave propagation programs were summarized to help identify the state of the art with respect to bridge pier analysis and to determine options for finding loading for the models. Research that examined different bridge pier column blast analysis methods was reviewed to determine common numerical simulation approximations along with parameters that have been traditionally examined to determine reinforced concrete, bridge pier column blast response. Several material models appropriate for blast loading on reinforced concrete were also summarized along with literature that examined which material models are most accurate for the steel reinforcement. Finally, current approaches for completing

simplified analyses of reinforced concrete, bridge pier columns under blast loads were reviewed and summarized.

Chapter 3

Simplified Numerical Bridge Model

This chapter discusses a simplified numerical bridge pier modeling method first proposed by Lobo (John Lobo, personal communication, Jan. 2012). The simplified numerical model was developed to be a conservative analysis tool to facilitate in the design of new bridge pier columns. One of the primary objectives of the current research is evaluation of the efficacy of this simplified numerical modeling approach.

Discussed herein are decisions and simplifications used to represent and apply the appropriate blast loading to the model. The simplified bridge model was developed so that bridge pier columns subjected to blast loads can be analyzed efficiently using commercially available structural analysis software. FEA and blast wave propagation programs are not readily available to many engineers, therefore complex models are not feasible. In addition, more advanced models are not always warranted due to the large uncertainty associated with the size and location of the explosives. This simplified bridge model was developed to provide accurate results without the time requirements associated with more sophisticated models.

3.1 Simplified Bridge Numerical Model

The developed simplified bridge model utilizes a MDOF, uncoupled analysis that can be completed using commercially available structural analysis software. The uncoupled analysis requires two analysis steps: 1) determine the loads on the structure; and 2) determine the response of the structure.

A single bridge pier column is modeled because it is assumed that other columns do not appreciably affect the response of that column. This is a common assumption when modeling blast loads on bridge pier columns because pressure waves that are reflected off adjacent columns are not significant compared to the incident pressure waves (Winget et al., 2005). The mass of the superstructure is concentrated at the top of the column, discrete masses are defined along the column length, and the base of the column is assumed to be fixed. The point of fixity is at the base of the column for columns supported on either spread footings or pile caps. For the case of columns supported by a single drilled shaft, the point of fixity is at a depth of approximately three shaft diameters below the base of the column. This approximation accounts for the interaction of the column and the drilled shaft and is based on the depth to fixity prescribed in *AASHTO LRFD Bridge Design Specifications* (2012).

The top of the column may be treated as fixed against translation in a direction parallel to the longitudinal axis of the bridge for multi-span continuous superstructures with loads parallel to the bridge axis. For loads perpendicular to the bridge axis of the bridge, the top of the column is free to rotate and translate.

3.2 Blast Loads

The explosion is assumed to take place at or close to the ground surface, which would represent explosives inside a small vehicle. Therefore, given the proximity of the explosion to the ground it is treated as a surface blast. The blast loads on the column are calculated from CONWEP, which is also used in the LS-DYNA FEM. The blast loads could also be calculated using other software or UFC 3-340-02 (2008).

Blast loads are applied to the column by multiplying the peak positive incident pressure by the diameter of the column, which is assumed to be the projected surface width of a circular column, to calculate the distributed load along the height of the column. In the case of a rectangular column, the pressures are multiplied by the column width. The distributed load is then multiplied by four equal tributary areas to obtain a series of four equally spaced point loads along the column height. The column is divided into four lumped masses where the point loads are applied. The mass of the superstructure is lumped into the top mass, M, as shown in Figure 3-1. The stiffness of the linear connecting elements, k_i, represent the stiffness of the column. The stiffness magnitude is calculated by the respective compute programs based on material and geometry properties.

3.3 Analysis

To complete a time-history analysis of the column under blast loads a program such as SAP2000 is employed. Time-history analyses are completed step wise to elicit the dynamic response of a structure under specified loads that vary with time. Several time-history analysis options are available in SAP2000: linear or nonlinear; modal or direct integration; and transient or periodic. Both material and geometric nonlinearities can be accounted for when completing any of the available SAP2000 time-history analyses.

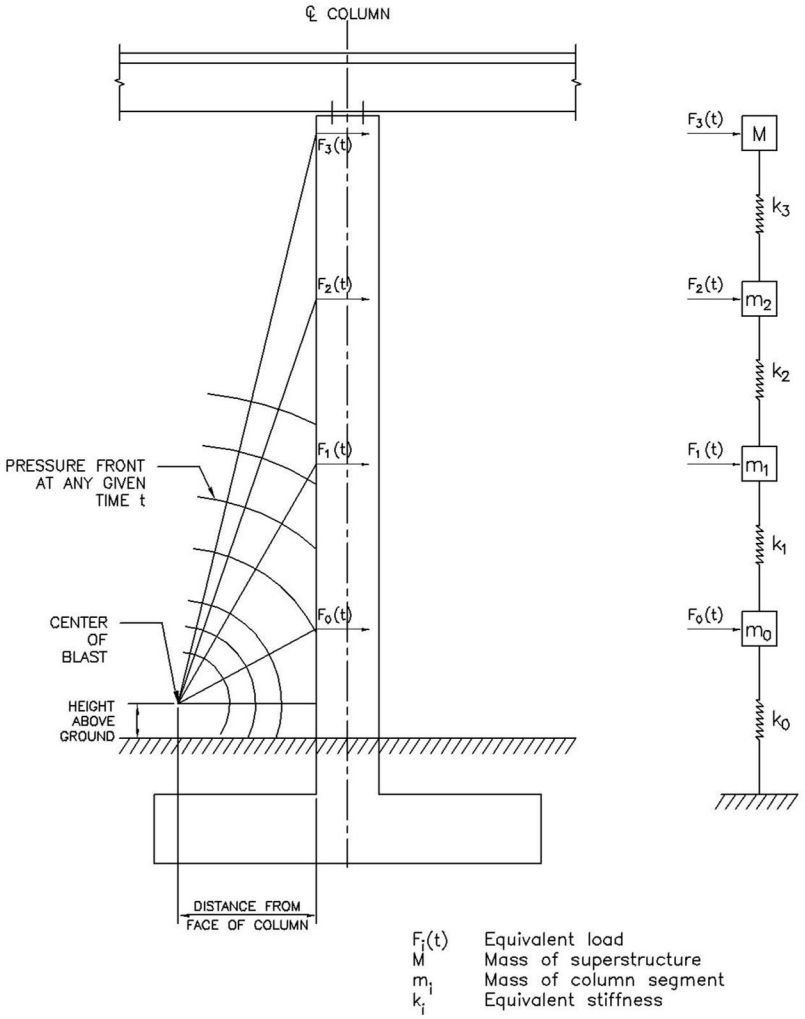

Figure 3-1 Simplified Model Schematic

A time-history analysis using modal superposition uses closed-form integration of the modal equations to compute the structure response. Modal superposition assumes linear variation of the time functions between the input points. In SAP2000, modal superposition is designed for structural systems that are primarily linearly elastic, but have a limited number of predefined nonlinear elements. Modal superposition is usually more accurate and efficient than direct integration, but direct integration of the equations of motion can account for all contributing nonlinearities.

A transient analysis has a one-time applied load, where a periodic analysis considers the load to repeat indefinitely with all transient response damped out.

The analysis that will be completed in SAP2000 in this study is a linear time-history analysis using modal superposition.

3.4 Summary

Presented in this chapter are approximations and a modeling methodology to accomplish the simplified bridge numerical model that is being evaluated in this study. Included are the decisions and simplifications used to efficiently model a bridge column under blast loads. The determination of loads and selection of an analysis method are also discussed. The method investigated utilizes MDOF, uncoupled analysis and incorporates approximations related to the structure being examined and its boundary conditions, lumped masses, and loads. The method aims to be economically efficient in terms of time and conservatism and is intended to be used with commercially available software.

Chapter 4

LS-DYNA Finite Element Model

High level FEMs were developed in LS-DYNA to complete a parametric study that helps to establish the effectiveness and limitations of the modeling approach summarized in Chapter 3. A bridge column is modeled subject to a blast load to represent the most critical structural component during a ground blast event. The model is composed of continuum elements with distributed mass and stiffness throughout the column. Nonlinear geometry and materials are considered in the explicit dynamic analysis. For this type of event, a particular interest is the concrete material modeling which incorporates degradation and failure.

This chapter presents element types, boundary conditions, element constraints, coupling techniques, material models, loads, and analysis techniques that will be used for finite element models investigating the performance of bridge pier columns under blast loads. LS-DYNA was selected for the present study because of its proven effectiveness for modeling structures under blast loads (NCHRP, 2010; LSTC, 2014) and because the blast wave propagation program CONWEP is incorporated into its capabilities.

4.1 Finite Elements

LS-DYNA models utilize constant stress solid elements to model the concrete. The Hughes-Liu beam element was used to model the steel reinforcement. Figure 4-1a) and b) show the parts used in LS-DYNA for the concrete and reinforcement. Figure 4-2 a), b), and c) show the concrete and reinforcement mesh.

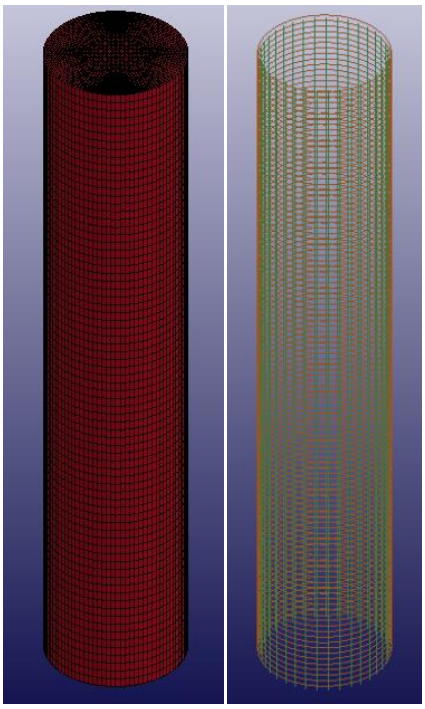

a. **b.**

Figure 4-1 Representative LS-DYNA Pier Column Parts: a.) Concrete; b.) Reinforcement

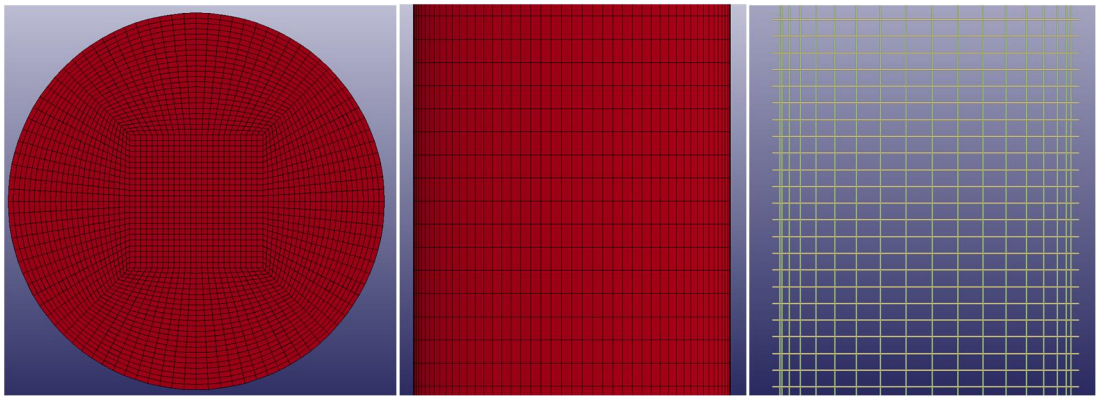

a. b. c.

Figure 4-2 LS-DYNA Mesh a) Cross-section, b) Concrete, c) Reinforcement

4.2 Boundary Conditions

Three boundary condition cases were modeled for the studied pier columns. The first case was a propped cantilever based on common bridge column blast research assumptions. This case represents girders as simply supported, which provides longitudinal translation restraint in a direction parallel to the bridge axis. The propped

cantilever was defined in LS-DYNA by fixing all nodes on the base of the column against translation and rotation in each direction. The nodes at the top of the column were fixed against translation parallel to the direction of the blast pressure. The second case was a pure cantilever. This support condition was modeled to investigate the effects of ignoring superstructure stiffness on simplified model accuracy by examining situations that place the greatest shear demand at the base of the column. The pure cantilever was defined in LS-DYNA by fixing all nodes on the base of the column against translation and rotation in each direction. The third case included construction joints at the column base based on research by O'Hare (2011), which indicated that modeling construction joints at the base of the column gives more accurate results when compared to experimental, pier column air blast test data. The construction joint at the base of the column was defined in LS-DYNA using the Contact Nodes to Surface function discussed in Section 4.3. The three boundary conditions are presented in Figure 4-3.

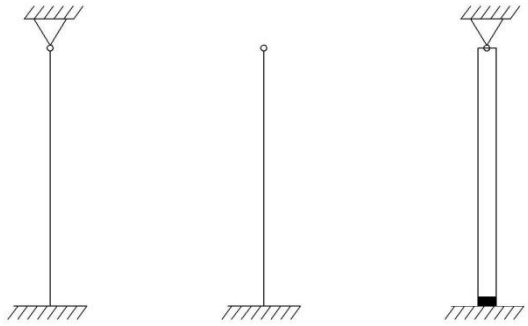

Figure 4-3 Boundary Conditions, a) Propped Cantilever, b) Free Cantilever, c) Construction Joint at Base of Column

4.3 Element Constraints/Coupling

Elements can be constrained or coupled using three different methods in LS-DYNA. They include nodal compatibility; the Constrained Lagrange in Solid LS-DYNA function; and the Nodes to Surface LS-DYNA function (LSTC, 2014).

Nodal compatibility is used to couple elements that are located in close proximity to each other and assumes complete coupling between the connected elements. To use nodal compatibility, common nodes need to be established within the bridge pier column. For example, the nodes shown in Figure 4-4 do not align and the elements are not coupled. For these elements to have nodal compatibility, the elements must have nodes that are aligned such as the nodes shown in Figure 4-5. Nodal compatibility is widely accepted in computational research, but can sometimes create too many elements, meshing complexity and increase the analysis time (O'Hare 2011).

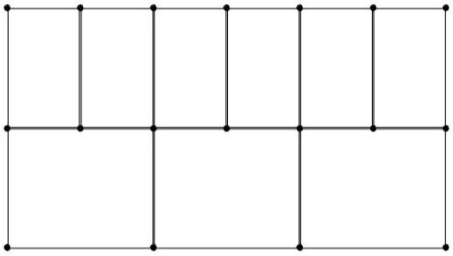

Figure 4-4 Elements without Nodal Compatibility

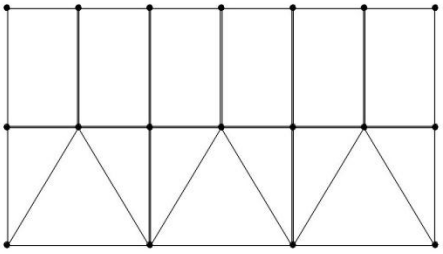

Figure 4-5 Elements with Nodal Compatibility

The Constrained Lagrange in Solid LS-DYNA function is another method that can be used to constrain degrees of freedom to move together. For this study, it was used to embed and couple reinforcement beam elements in concrete solid elements. The beam elements are defined as a set of Lagrangian, or deformable mesh, slave parts that are coupled to a defined set of master parts, representing the concrete, at the nodes via velocities and accelerations (LSTC, 2014). As presented in Figure 4-6, the longitudinal and transverse reinforcement is embedded in the concrete and the reinforcement is constrained to the concrete using the LS-DYNA function.

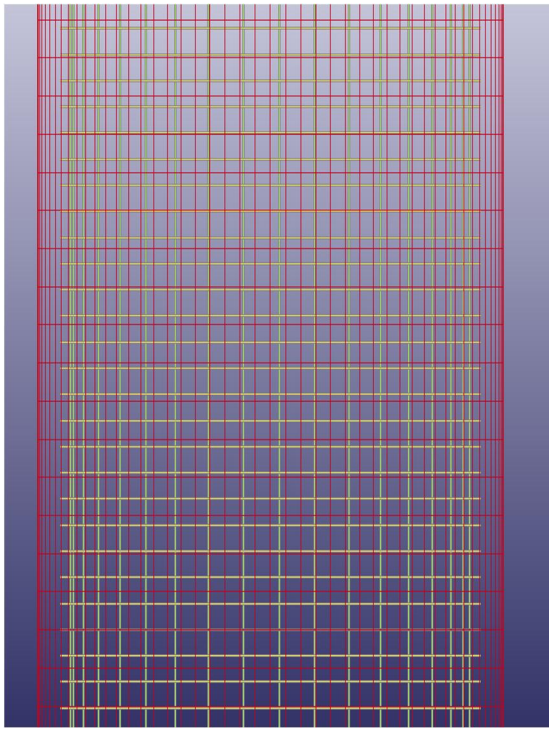

Figure 4-6 LS-DYNA Constrained Lagrange in Solid Definition

The Contact Nodes to Surface LS-DYNA function is a method to couple elements together by treating interaction between two LS-DYNA parts, which are defined to encompass material information and section properties to elements they contain. For this study, it was used when modeling the construction joint at the base of the column at the

top of the footing surface, which has been reported to provide a more accurate representation of bridge pier boundary conditions when compared to experimental results.

The footing will be modeled as a rigid surface to reduce computation time as recommended by O'Hare (2011). This contact definition prevents a set of slave nodes from penetrating the set of master segments in compression. In tension, the slave nodes are allowed to pull away from the master segments. The slave nodes are nodes at the base of the column, and the master segments are on the top face of the footing and, as a result, the base of the column can pull away from the footing but not penetrate the footing, thereby mimicking a construction joint between the column and footing. Reinforcement between the column and footing was modeled to provide tension and shear capacity across the joint that would exist in an actual column. A friction coefficient for concrete on concrete was defined in the Contact Nodes to Surface LS-DYNA function at the interface to represent friction resistance that would occur at the column base.

4.4 Material Models

Material type 159 was used for the concrete in this research based on work by O'Hare (2011), which showed that blast loaded bridge pier columns were accurately modeled using this material model when compared to experimental results.

Material type 3 was used in this study for the steel reinforcement based on recommendations by O'Hare (2011).

4.5 Blast Loads

The empirically based blast load function code, CONWEP, which is integrated into LS-DYNA as discussed in Chapter 2, was used in this study to generate the blast loads on the column. CONWEP calculates the loads on a structure for a given amount of TNT at a given distance. For this study, a charge weight of 500 lb. of TNT was used with standoff distances of 1.2 meters (4.0 feet) and 7.6 meters (25.0 feet). CONWEP calculated a pressure-time history in terms of an incident pressure, reflected pressure, and angle of incidence.

4.6 Analysis Method

LS-DYNA was selected for the present study because of its proven effectiveness for modeling structures under blast loads (NCHRP, 2010; LSTC, 2014) and because the blast wave propagation program CONWEP is incorporated into its capabilities. LS-DYNA was used to complete an explicit, dynamic time-history analysis. A time-history analysis gives the response of the structure during and after the application of the blast load. An explicit analysis refers to the numerical method used to predict the solution. An explicit analysis calculates displacements and velocities in terms of quantities that are none at the beginning of the time step. It uses the solution at time t to predict the solution at time $t+\Delta t$. An explicit analysis is computationally efficient, but conditionally stable so the time step, Δt, must be less than a critical value. The critical time step is calculated in LS-DYNA with Equation (4-1).

$$\Delta t_{cr} = \frac{V_e}{C A_{e,\max}} \tag{4-1}$$

where: V_e is the element volume, $A_{e,max}$ is the area of the largest side of the element, and C is the plane stress sound speed which is calculated using Equation (4-2).

$$C = \sqrt{\frac{E}{p\left(1-v^2\right)}} \tag{4-2}$$

where: E is Young's modulus, p is the specific mass density, and v is Poisson's ratio. The time step used in LS-DYNA is equal to $0.67\Delta t_{cr}$ (LSTC, 2014). The explicit analysis runs in LS-DYNA until the termination time is reached. For the present study, the termination time was set to 0.25 seconds.

4.7 Summary

This chapter summarized available element types and coupling methods in LS-DYNA. The boundary conditions, loads, and analysis technique that were used in this study are also summarized. Finite element types that were used in this research are solid and Hughes-Liu beam elements for the concrete and steel, respectively. Three column boundary conditions cases were examined. The first case was a propped cantilever based on commonly reported blast analysis approaches for bridge pier columns. The second case was a pure cantilever that produces the highest shear demand at the base of the column. The third case included construction joints at the base of the column based on research that indicated modeling the construction joints gives more accurate results when compared to experimental data. The three different types of constraints that were used in this study to model these boundary conditions are nodal compatibility, the *CONSTRAINED_LAGRANGE_IN_SOLID LS-DYNA function, and the *CONTACT_NODES_TO_SURFACE LS-DYNA function. LS-DYNA Material Type

159 was used to model the concrete and Material Type 3 was used for the reinforcement. The loads on the column were determined from the blast propagation program CONWEP, which is incorporated into LS-DYNA. The LS-DYNA analysis technique that was used is a MDOF coupled approach involving an explicit, dynamic, time-history analysis.

Chapter 5

Numerical Simulation Parametric Studies

This chapter details the parametric studies that were used to evaluate the effectiveness of the simplified numerical simulation approach described in Chapter 3 and to establish limits for its application. This study examines the effects of several factors on the results, therefore a 2^k factorial design was selected. In general, factorial designs an efficient method for completing studies that examine the effects of two or more factors on a response (Montgomery, 2009). Factorial designs determine the effect of several factors on the response rather than one factor at a time. Factorial designs examine all possible combinations of parameter levels. A 2^k factorial design has two levels of *k* parameters. The levels can be quantitative or qualitative and are commonly minimum and maximum values.

Important study variables that were kept constant are summarized here and their values justified. In addition, parameters that were varied are presented and justified along with their minimum and maximum values.

5.1 Constants

NCHRP Report 645 (NCHRP, 2010) included a survey of state DOTs to identify several common bridge pier column parameters throughout different states. Parameters highlighted in this survey that were not varied for the present study include: column geometry (circular), concrete compressive strength (f'_c) of 27.6 MPa (4,000 psi) and A615 Gr. 60 steel reinforcing bars. A concrete cover of 51 mm (2″) on the reinforcement

was used in NCHRP Report 645, but 76 mm (3″) concrete cover is used in this study to reflect what is used in Arizona.

The pre-compression load, which represents the axial load from the superstructure on the column, are also constant. Priestley et al. (1994) demonstrated that typical axial loads on bridge pier columns range from $0.06(f'_c A_g)$ to $0.18(f'_c A_g)$, where f'_c is the 28 day compressive strength of the concrete and A_g is the cross-sectional area of the column. This study will use $0.12(f'_c A_g)$ as the preload on the column because it is the mean of values identified by Priestley et al. (1994).

The transverse reinforcement type and ratio are constant in this study. Discrete hoops are used. The minimum transverse reinforcement ratio for typically designed circular columns is given in Equation (5-1) (AASHTO, 2007):

$$\rho_s \geq 0.45\left(\frac{A_g}{A_c} - 1\right)\frac{f'_c}{f_y} \tag{5-1}$$

where: A_g = gross area of the column; A_c = area of the concrete core; f'_c = compressive strength of concrete at 28 days; and f_y = yield strength of reinforcing bars.

Equation (5-2) details the minimum transverse reinforcement ratio from the seismic provisions of AASHTO (2012):

$$\rho_s \geq 0.12\frac{f'_c}{f_y} \tag{5-2}$$

NCHRP Report 645 used the higher minimum reinforcement ratio for blast loaded columns from Equation (5-3) to investigate the effect on column strength, ductility and energy dissipation:

$$\rho_s \geq 0.18\frac{f'_c}{f_y} \tag{5-3}$$

This study uses a transverse reinforcement ratio that is the greatest of those produced from Equations (5-1), (5-2), and (5-3). The constant parameters are summarized in Table 5-1.

Table 5-1 Summary of Constant Parameter Values

Constant Parameter	Parameter Value
Column Geometry	Circular
Compressive strength of concrete (f'_c)	27.57 MPa (4,000 psi)
Yield strength of reinforcement (f_y)	A615 Grade 60
Concrete cover	76 mm (3 inches)
Axial load	$0.12(f'_c A_g)$
Transverse reinforcement ratio	Maximum of $\rho_s \geq 0.45\left(\frac{A_g}{A_c} - 1\right)\frac{f'_c}{f_y}$ and $\rho_s \geq 0.18\frac{f'_c}{f_y}$

5.2 Varied Parameters

The following parameters were varied for this study: column aspect ratio; column longitudinal reinforcement ratio; column boundary conditions; and the scaled distance used to represent the blast load. These parameters were selected as variables because they are anticipated to be the most critical with respect to the performance of bridge columns under blast loads, and a summary of their limits is provided in Table 5-2.

Table 5-2 Summary of Varying Parameter Limits

Parameter	Minimum	Maximum
L/d	5	11
ρ	1%	2%
BCs	Propped cantilever	Construction joint at base of column
Z	0.198 m/kg$^{1/3}$ (0.5 ft/lbm$^{1/3}$)	1.25 m/kg$^{1/3}$ (3.15 ft/lbm$^{1/3}$)

5.2.1 Column Aspect Ratio

The column aspect ratio, *L/d*, was varied between 5 and 11 based on practical column dimensions supplied by Lobo (John Lobo, personal communication, Jan. 2012). *L* is the length of the column and *d* is the diameter of the column as presented in Figure 5-1. The aspect ratio is important for blast loaded columns because it is related to column lateral stiffness and shear capacity. The diameter of the cross-section is directly related to the shear capacity of the column. AASHTO shear provisions are to determine the shear reinforcement of the column based on a given cross-section size. For this study the column diameter was kept constant at 1524 mm (60″) while varying the column height to obtain *L/d* ratios of 5 and 11. A cross-section of the column is presented in Figure 5-2.

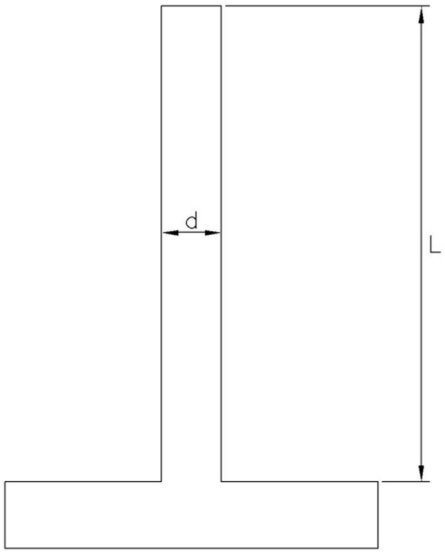

Figure 5-1 Column Height and Diameter

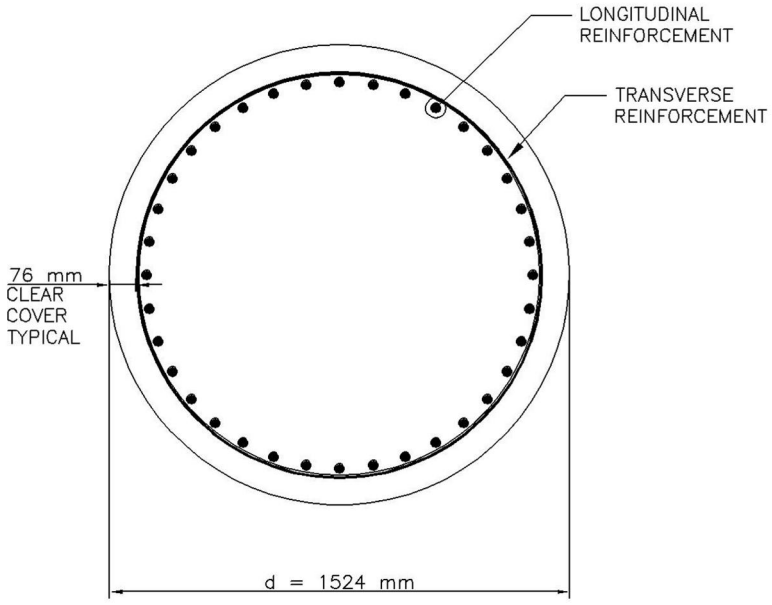

Figure 5-2 Column Cross-Section

5.2.2 Longitudinal Reinforcement Ratio

A longitudinal reinforcement ratio of 1% and 2% was used based on practical column designs. AASHTO specifies the maximum ratio of longitudinal reinforcement for noncomposite compression components as 8%.

Equation (5-4) specifies the minimum area of longitudinal reinforcement for noncomposite compression components (AASHTO, 2012).

$$\frac{A_s f_y}{A_g f'_c} \geq 0.135 \tag{5-4}$$

These limits are used to determine the maximum and minimum area of reinforcement allowed by AASHTO (2012). Specified 1% and 2% reinforcement ratios fit within the acceptable range specified in AASHTO (2012).

5.2.3 Boundary Conditions

Three boundary conditions of the column were examined as discussed in Chapter 4. They include a propped cantilever, a pure cantilever, and a model that includes the construction joint at the base of the column.

5.2.4 Standoff Distance

The equations in the LS-DYNA blast load function are limited to scaled distances between 0.054 and 39.7 m/kg$^{1/3}$ (0.136 and 100 ft/lbm$^{1/3}$) (LSTC, 2014). As shown in Equation (2-2), the scaled distance is calculated as a function of the distance from the center of the explosion and the weight of the explosive in TNT equivalence. For the present study the weight of standard explosive, *W*, was held constant and the distance from the center of the explosion, *R*, was varied. The equivalent weight of TNT, *W*, is 230 kg (500 lb) based on the maximum value for automobiles from Table 3 of the *Recommendations for Bridge and Tunnel Security* (FHWA, 2003). The actual standoff distance for the charge will be either 1.2 meters (4.0 feet) or 7.6 meters (25.0 feet). The scaled distances, *Z*, are calculated as follows:

$$Z = \frac{R}{W^{1/3}} = \frac{1.2\text{m}}{(230\text{kg})^{1/3}} = 0.198 \text{ m/kg}^{1/3}$$

The scaled distances used in the present study are 0.198 m/kg$^{1/3}$ (0.5 ft/lbm$^{1/3}$) and 1.25 m/kg$^{1/3}$ (3.15 ft/lbm$^{1/3}$). These standoff distances were selected to represent a close-in standoff distance and a faraway distance for actual bridge pier columns. The close-in distance was selected because existing research determined that a vehicle cannot be closer than 1.2 meters to a bridge column (Islam and Yazdani, 2008). The far distance was selected as 7.62 meters because standoff distances larger than 7.62 meters have been

shown to produce negligible loads for a charge weight of 500 lb of TNT (Islam and Yazdani, 2008).

5.3 Summary

This chapter details the parameters used in the present study and the conduct of the parametric study to determine the effectiveness and limitations of the simplified bridge numerical simulation. Constants and parameters were presented along with justification behind values that were chosen. A 2^k factorial design was used to evaluate each of the parameters at combinations of their minimum and maximum values.

The parametric study was completed by running a model with each set of parameters in LS-DYNA and SAP2000. This resulted in twenty-four (24) LS-DYNA models and sixteen (16) SAP models. A list of all of the numerical simulation models created in this study is shown in Table 5-3. After all of the models were run, models were grouped together with like aspect ratios, longitudinal reinforcement ratios, and scaled distances but with varied boundary conditions. The models were grouped together as shown in Table 5-4. All groups have the following five models: propped cantilever in LS-DYNA; propped cantilever in SAP2000; construction joint at base of column in LS-DYNA; free cantilever in LS-DYNA; and free cantilever in SAP2000.

Table 5-3 List of all Finite Element and Simplified Models

Model #	*L/d*	Boundary Condition	ρ (%)	Z (m/kg$^{1/3}$)	FEA	Simplified
1	5	Propped Cantilever	1	0.198	LS-DYNA	SAP
2	5	Propped Cantilever	1	1.25	LS-DYNA	SAP
3	5	Propped Cantilever	2	0.198	LS-DYNA	SAP
4	5	Propped Cantilever	2	1.25	LS-DYNA	SAP
5	5	Construction joints	1	0.198	LS-DYNA	-
6	5	Construction joints	1	1.25	LS-DYNA	-
7	5	Construction joints	2	0.198	LS-DYNA	-
8	5	Construction joints	2	1.25	LS-DYNA	-
9	11	Propped Cantilever	1	0.198	LS-DYNA	SAP
10	11	Propped Cantilever	1	1.25	LS-DYNA	SAP
11	11	Propped Cantilever	2	0.198	LS-DYNA	SAP
12	11	Propped Cantilever	2	1.25	LS-DYNA	SAP
13	11	Construction joints	1	0.198	LS-DYNA	-
14	11	Construction joints	1	1.25	LS-DYNA	-
15	11	Construction joints	2	0.198	LS-DYNA	-
16	11	Construction joints	2	1.25	LS-DYNA	-
17	5	Free cantilever	1	0.198	LS-DYNA	SAP
18	5	Free cantilever	1	1.25	LS-DYNA	SAP
19	5	Free cantilever	2	0.198	LS-DYNA	SAP
20	5	Free cantilever	2	1.25	LS-DYNA	SAP
21	11	Free cantilever	1	0.198	LS-DYNA	SAP
22	11	Free cantilever	1	1.25	LS-DYNA	SAP
23	11	Free cantilever	2	0.198	LS-DYNA	SAP
24	11	Free cantilever	2	1.25	LS-DYNA	SAP

Table 5-4 Model Groupings

Group Number	*L/d*	ρ (%)	Z (m/kg$^{1/3}$)
1	5	1	0.198
2	5	1	1.25
3	5	2	0.198
4	5	2	1.25
5	11	1	0.198
6	11	1	1.25
7	11	2	0.198
8	11	2	1.25

Chapter 6

Numerical Simulation Results

This chapter presents the results from the parametric study that was completed using LS-DYNA and SAP2000. Pressure-time histories for the two scaled distances (Z = 0.198 kg/m$^{1/3}$ and 1.25 kg/m$^{1/3}$) are presented with the pressures from the simplified models and the LS-DYNA models. Moment envelopes, shear envelopes, and deflected shapes are presented for each group and the models are compared. The maximum moments and shear at each location are plotted. The deflected shapes presented are the deflected shape at the time of the maximum moment. There are 26 graphs presented to compare the simplified models to the LS-DYNA models. The results from SAP2000 are shown as dashed lines in the graphs and the results from the LS-DYNA models are shown as solid lines.

6.1 Blast Loading Comparison

The blast loads applied in the LS-DYNA and SAP models are presented in this section. The equivalent TNT weight and the location of the blast is input into LS-DYNA and CONWEP calculates the pressures applied to the column. In the simplified models, the peak pressure and time duration of the incident pressure from CONWEP were input into SAP2000. Therefore, the pressures in the SAP models and LS-DYNA models are approximately equal. The blast pressures for scaled distances, Z, of 0.198 kg/m$^{1/3}$ and 1.25 kg/m$^{1/3}$ are shown in Figures 6-1 and 6-2, respectively.

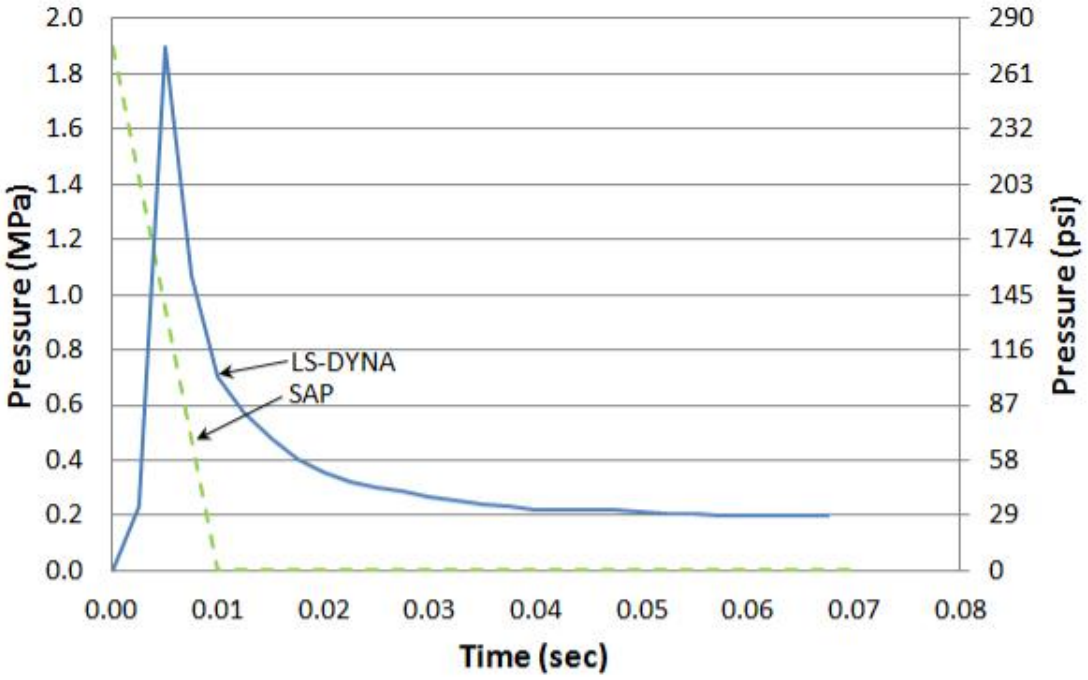

Figure 6-1 Pressure-Time History, Z = 0.198 kg/m$^{1/3}$

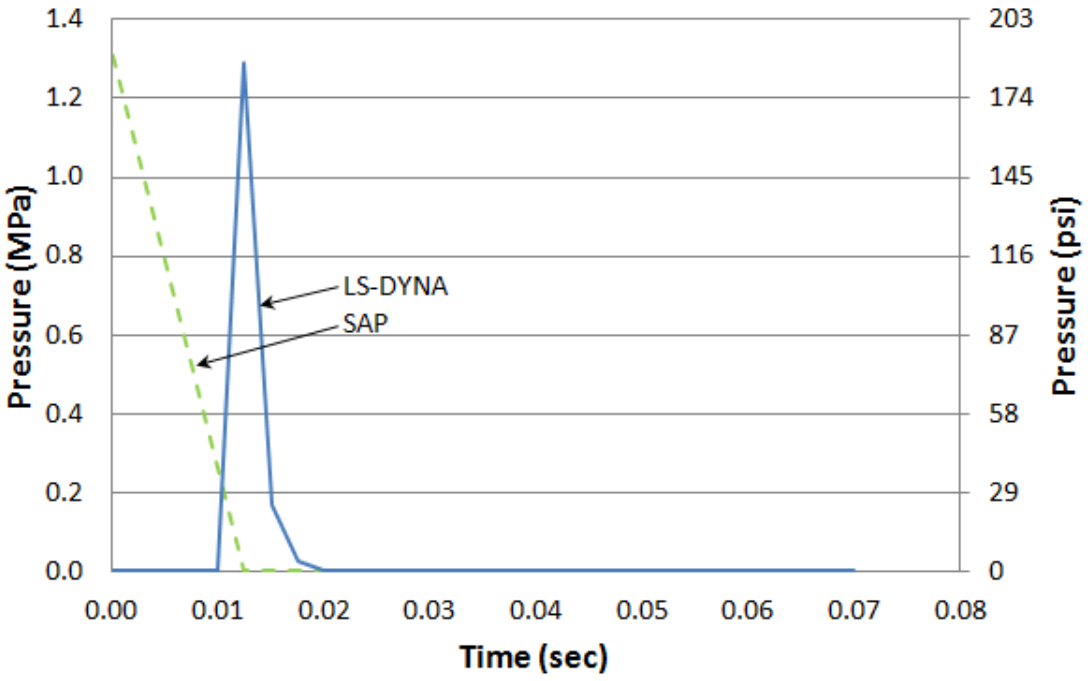

Figure 6-2 Pressure-Time History, Z = 1.25 kg/m$^{1/3}$

6.2 Group 1 Results

Group 1 models have the following parameters: column aspect ratio, *L/d*, of 5; longitudinal reinforcement ratio, ρ, of 1%; and a scaled distance, *Z*, of 0.198 kg/m$^{1/3}$ (0.5 ft/lbm$^{1/3}$). The moment envelope, shear envelope, and deflected shape are presented for group 1 models.

6.2.1 Group 1 Moment Envelope

The moment envelope for group 1 models is presented in Figure 6-3. From Figure 6-3 it can be observed that the two SAP models have very similar results. The moment at the base of the column and the maximum moments near mid-height of the column are the same values for both the propped cantilever and free cantilever SAP models. The moment at the base of the column from the SAP models is about twice as large as the LS-DYNA models. The maximum moment is between 3.8 m (12.5 ft) and 5.8 m (19.0 ft) from the base in the SAP models. However, the maximum moment in the LS-DYNA models is located between 4.5 m (14.75 ft) and 6.0 m (19.7 ft) from the base. The moments in the body of the column are typically 1.5 times larger in the SAP models than the LS-DYNA models.

6.2.2 Group 1 Shear Envelope

The shear envelope for Group 1 models is presented in Figure 6-4. From Figure 6-4, it can be observed that the two SAP models have very similar results. The propped and free cantilever SAP models have the same base shear and shear at the top of the column. The free cantilever has shear at the top of the column due to the discrete mass of the superstructure modeled at the top of the column. This is true for all of the free

cantilever SAP models. However, the free cantilever LS-DYNA model has zero shear at the top of the column. From the base of the column to approximately 4.5 m (14.75 ft) from the base the SAP models have higher shear than the LS-DYNA models. The shear at the top of the column in the SAP models is approximately 1.5 times larger than the shear in the LS-DYNA models.

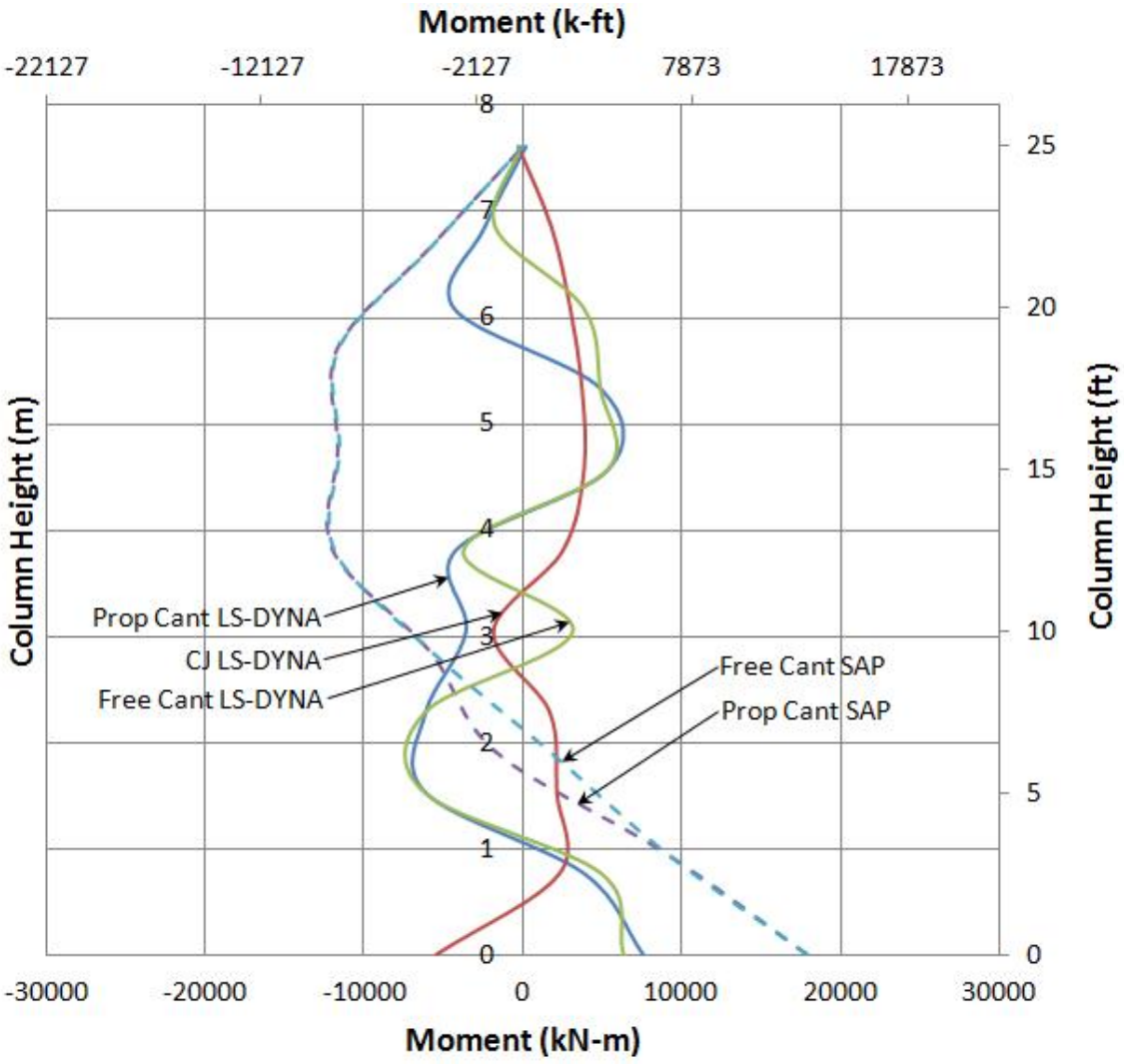

Figure 6-3 Moment Envelope, Group 1, L/d = 5, ρ = 1%, Z = 0.198 m/kg$^{1/3}$

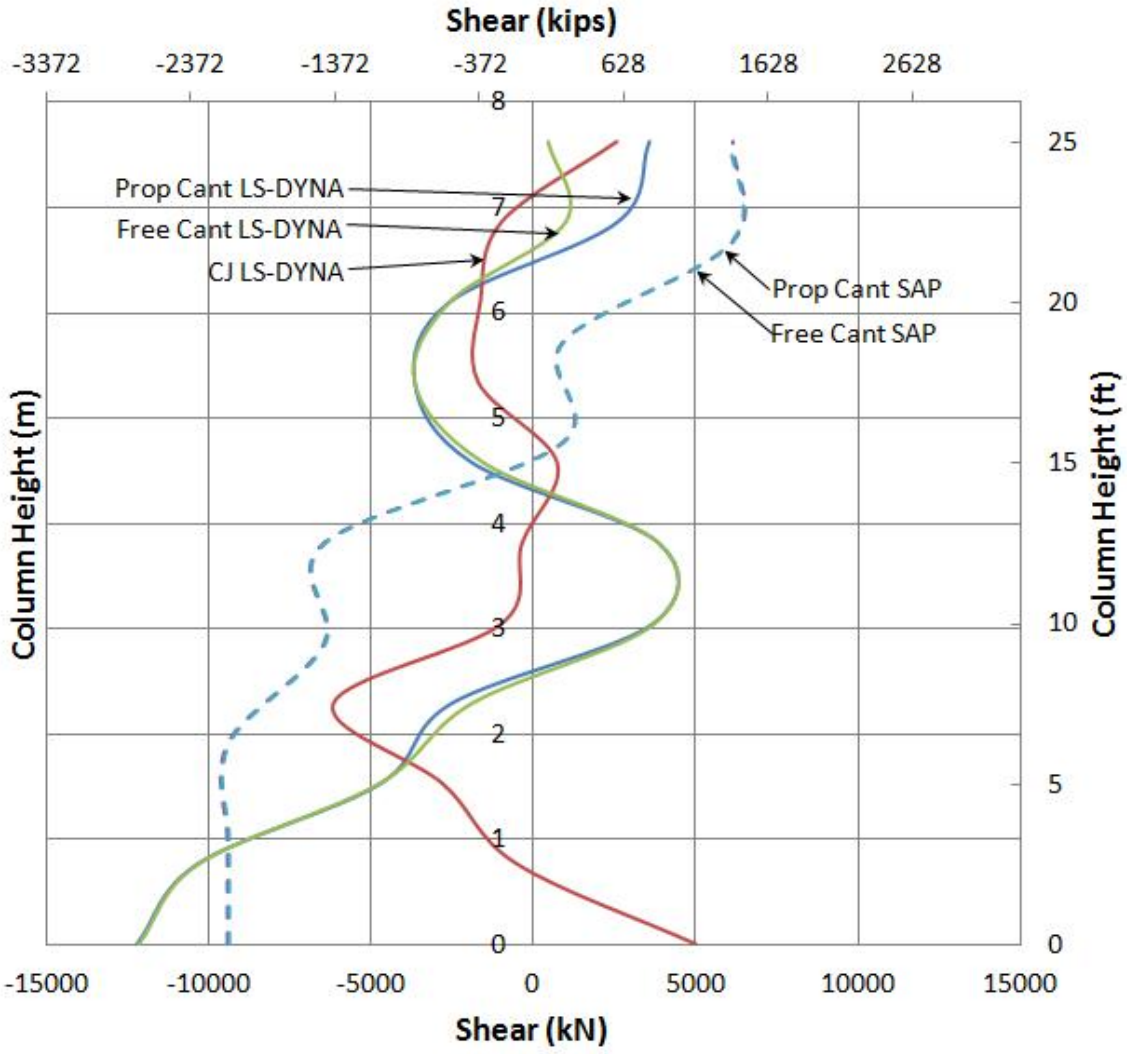

Figure 6-4 Shear Envelope, Group 1, L/d = 5, ρ = 1%, Z = 0.198 m/kg$^{1/3}$

6.2.3 Group 1 Deflected Shape

The deflected shape for Group 1 models is presented in Figure 6-5. From Figure 6-5 it can be observed that the two SAP models have similar deflected shapes except the free cantilever model has a small deflection at the top of the column. The free cantilever LS-DYNA model has a deflection at the top of the column about twice as large as the

free cantilever SAP model. The free cantilever and propped cantilever LS-DYNA models have approximately 1.25 times greater deflection at mid-height than the SAP models.

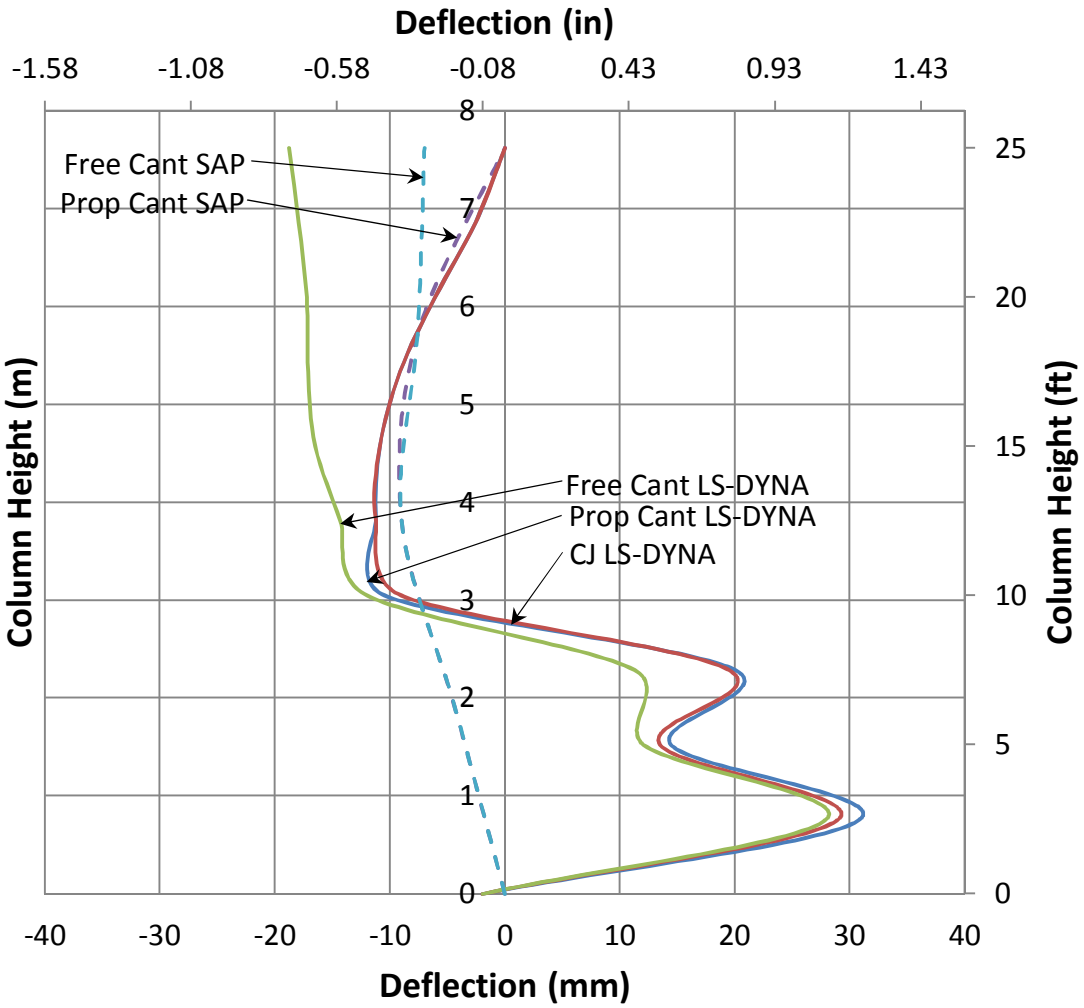

Figure 6-5 Deflected Shape, Group 1, L/d = 5, ρ = 1%, Z = 0.198 m/kg$^{1/3}$

6.3 Group 2 Results

Group 2 models have the following parameters: column aspect ratio, L/d, of 5; longitudinal reinforcement ratio, ρ, of 1%; and a scaled distance, Z, of 1.25 kg/m$^{1/3}$ (3.15

ft/lbm$^{1/3}$). The moment envelope, shear envelope, and deflected shape are presented for Group 2 models.

6.3.1 Group 2 Moment Envelope

The moment envelope for Group 2 models is presented in Figure 6-6. From Figure 6-6 it can be observed that the moment at the base of the column is about 3.5 times greater in the SAP models compared to the LS-DYNA models. All three LS-DYNA models have similar moments at the base of the column. The SAP models have approximately 2.5 times greater moments from approximately 1.8 m (5.9 ft) from the base to the top of the column compared to the moments from the LS-DYNA models.

6.3.2 Group 2 Shear Envelope

The shear envelope from Group 2 models is presented in Figure 6-7. It can be observed from Figure 6-7 that the SAP models have approximately 3 times larger shear at the base of the column compared to the propped cantilever and free cantilever LS-DYNA models. The propped cantilever and free cantilever SAP models have very similar results. The free cantilever SAP model has similar shear at the top of the column as the propped cantilever SAP model due to the discrete mass of the superstructure modeled at the top of the column. The shear at the top of the column in the SAP models is approximately 1.33 times greater than the propped cantilever LS-DYNA model and approximately 2 times greater than the construction joint LS-DYNA model.

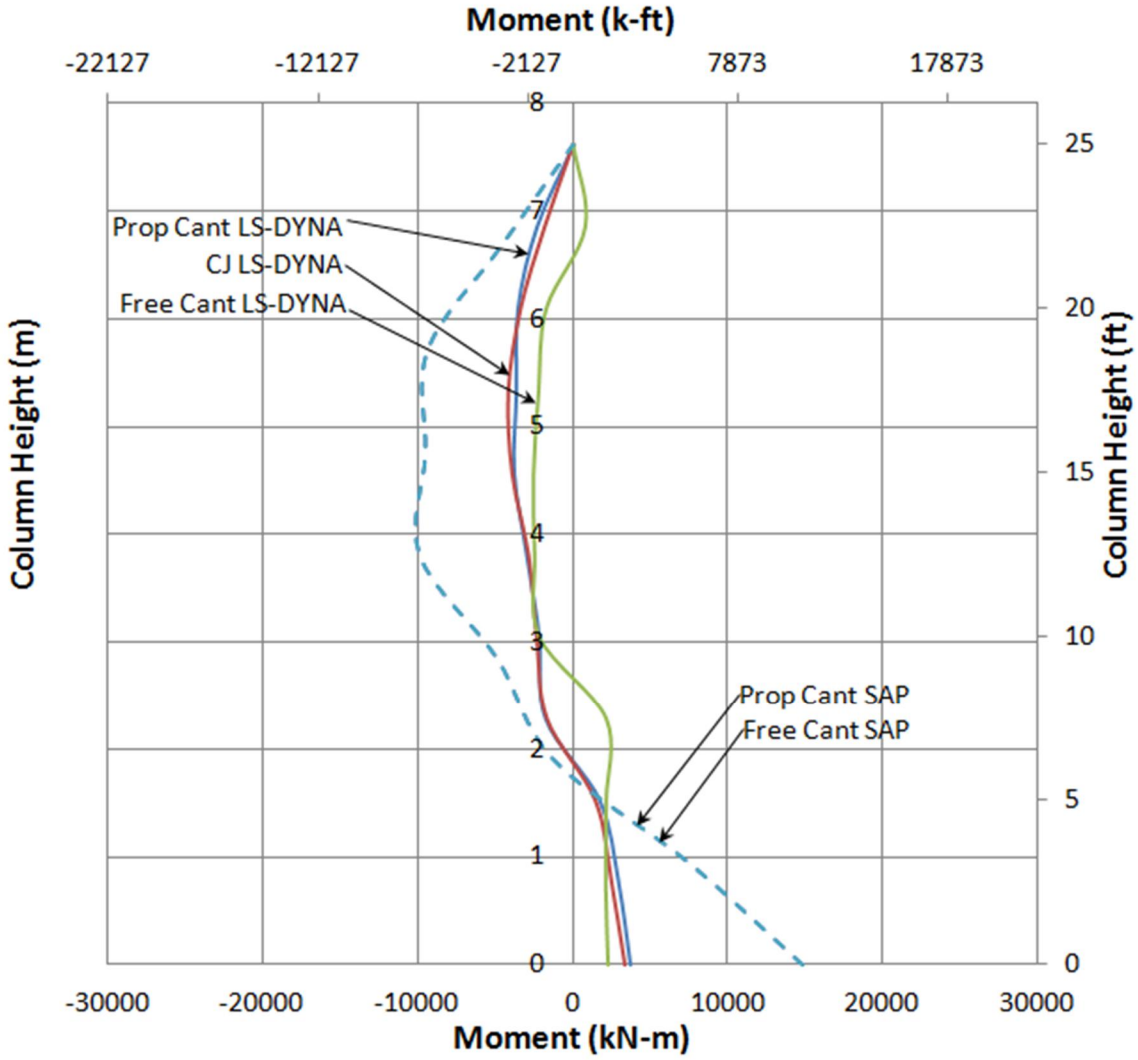

Figure 6-6 Moment Envelope, Group 2, L/d = 5, ρ = 1%, Z = 1.25 m/kg$^{1/3}$

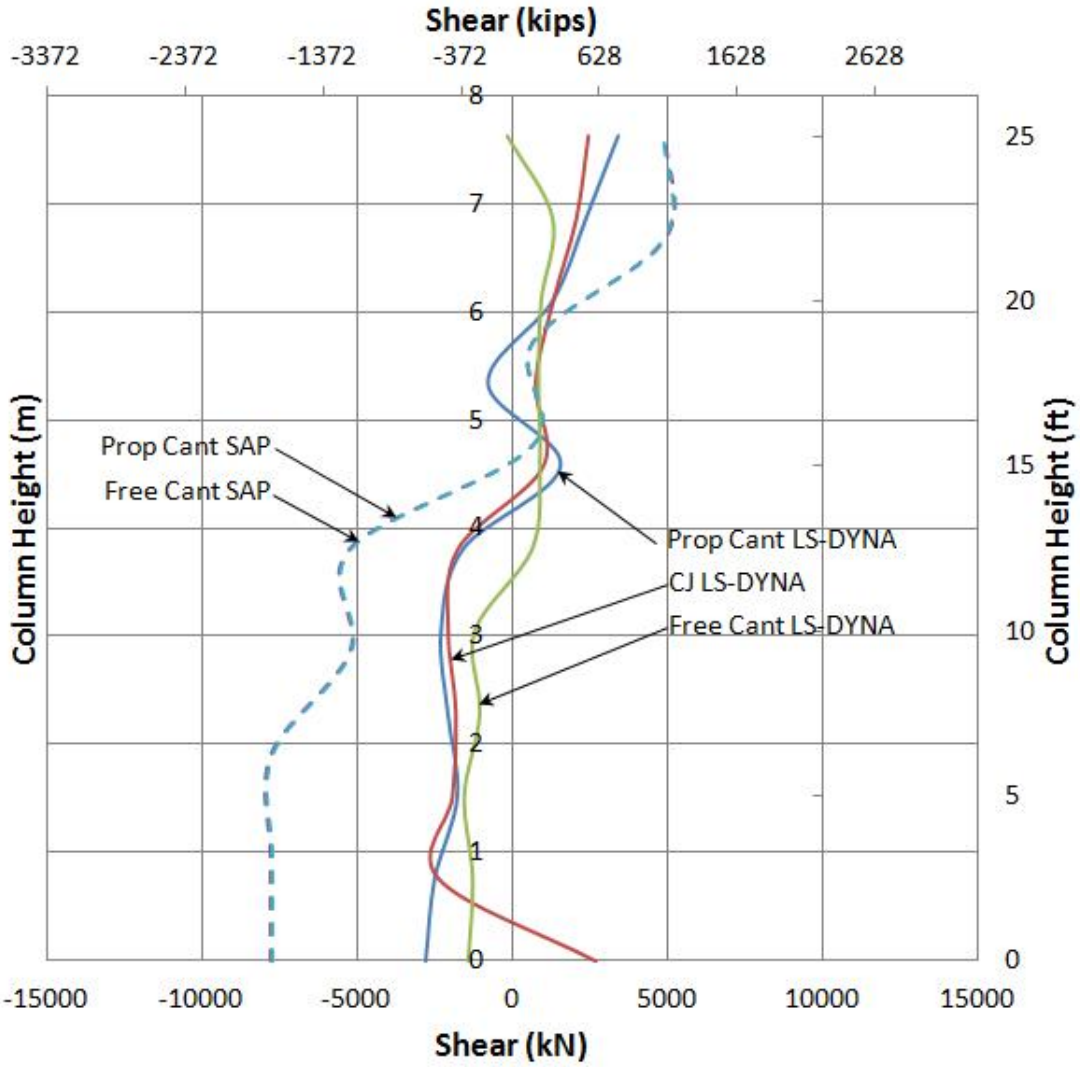

Figure 6-7 Shear Envelope, Group 2, L/d = 5, ρ = 1%, Z = 1.25 m/kg$^{1/3}$

6.3.3 Group 2 Deflected Shape

The deflected shape for Group 2 models is presented in Figure 6-8. As shown in Figure 6-8, the two SAP models have similar deflected shapes except for the top of the column. The deflection at the top of the column in the free cantilever LS-DYNA model is about 3.5 times greater than the deflection at the top of the free cantilever SAP model.

The deflection at mid-height of the SAP models is about 1.3 times greater than the propped cantilever and construction joint LS-DYNA models.

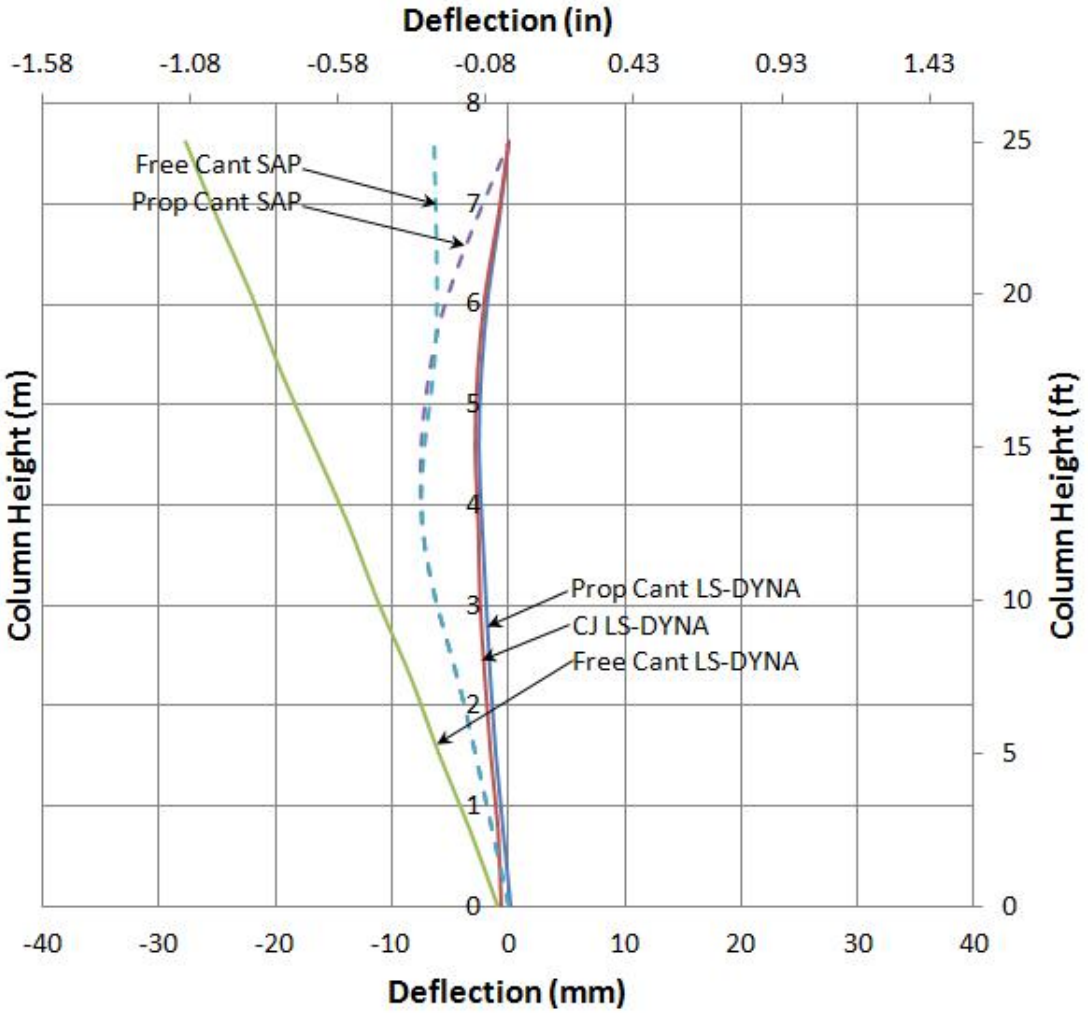

Figure 6-8 Deflected Shape, Group 2, L/d = 5, ρ = 1%, Z = 1.25 m/kg$^{1/3}$

6.4 Group 3 Results

Group 3 models have the following parameters: column aspect ratio, L/d, of 5; longitudinal reinforcement ratio, ρ, of 2%; and a scaled distance, Z, of 0.198 kg/m$^{1/3}$ (0.5 ft/lbm$^{1/3}$). The moment envelope, shear envelope, and deflected shape are presented for Group 3 models.

6.4.1 Group 3 Moment Envelope

The moment envelope for Group 3 models is presented in Figure 6-9.

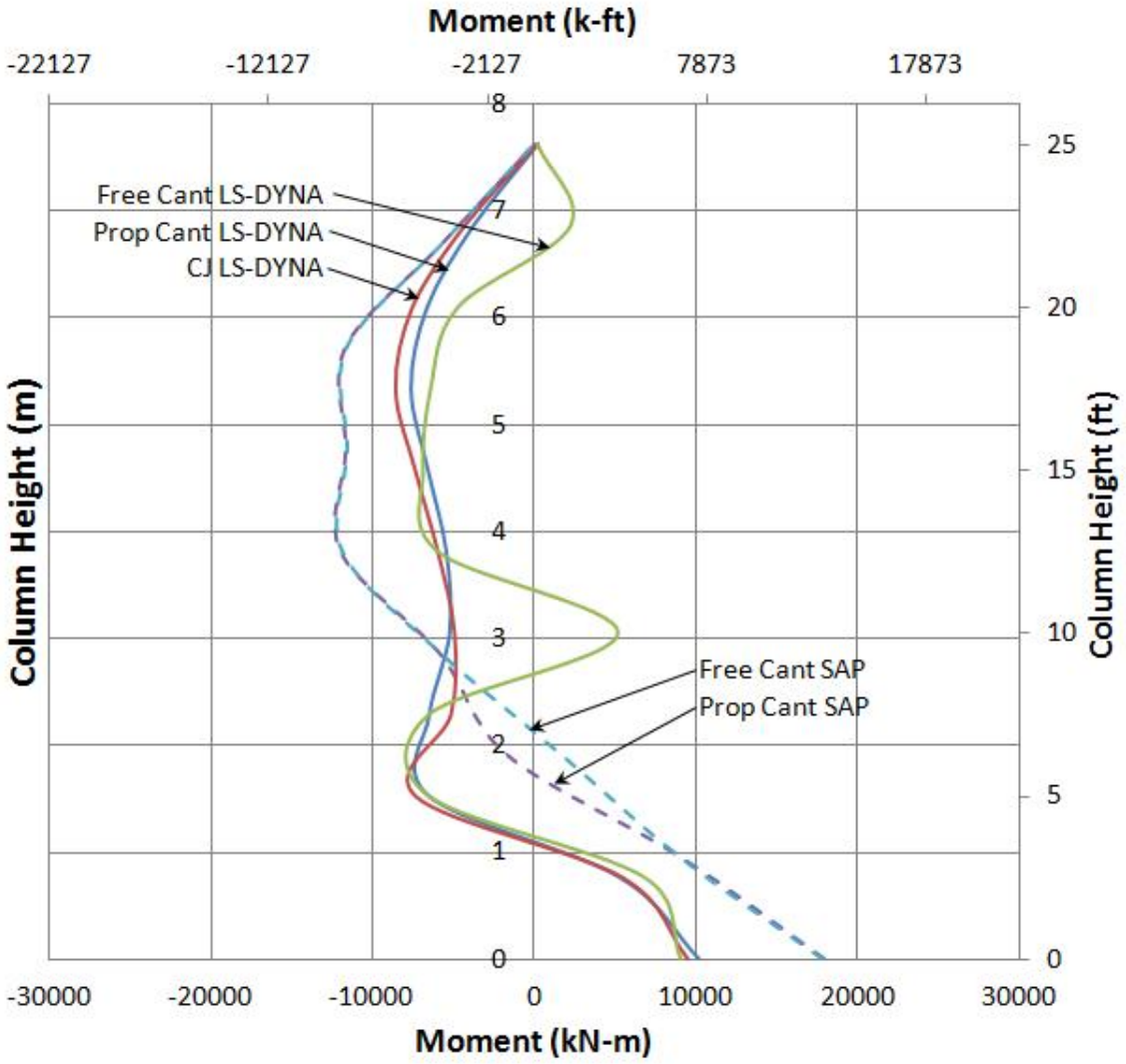

Figure 6-9 Moment Envelope, Group 3, L/d = 5, ρ = 2%, Z = 0.198 m/kg$^{1/3}$

From Figure 6-9 it can be observed that the moment at the base of the column is approximately 2 times larger in the SAP models than in the LS-DYNA models. The moments at the base of the column from the free cantilever and the propped cantilever LS-DYNA models are approximately the same. The moments in the SAP models are

approximately 1.5 times larger than the moments in the LS-DYNA models between 3500 mm (11.5 ft) and 6000 mm (19.7 ft).

6.4.2 Group 3 Shear Envelope

The shear envelope for the Group 3 models is presented in Figure 6-10. It can be observed from Figure 6-10 that the base shear in the propped cantilever and free cantilever LS-DYNA models is approximately 1.5 times greater than the base shear from the SAP models. The two SAP models have approximately equal shear envelopes. The free cantilever SAP model has shear at the top equal to the propped cantilever SAP model due to the discrete mass of the superstructure modeled at the top of the column. The SAP models and the propped cantilever and construction joint LS-DYNA models have approximately equal shear at the top of the column. The shear in the column is higher in the SAP models for the bottom half of the column. The shear in the column is higher in the LS-DYNA models for the top of half of the column.

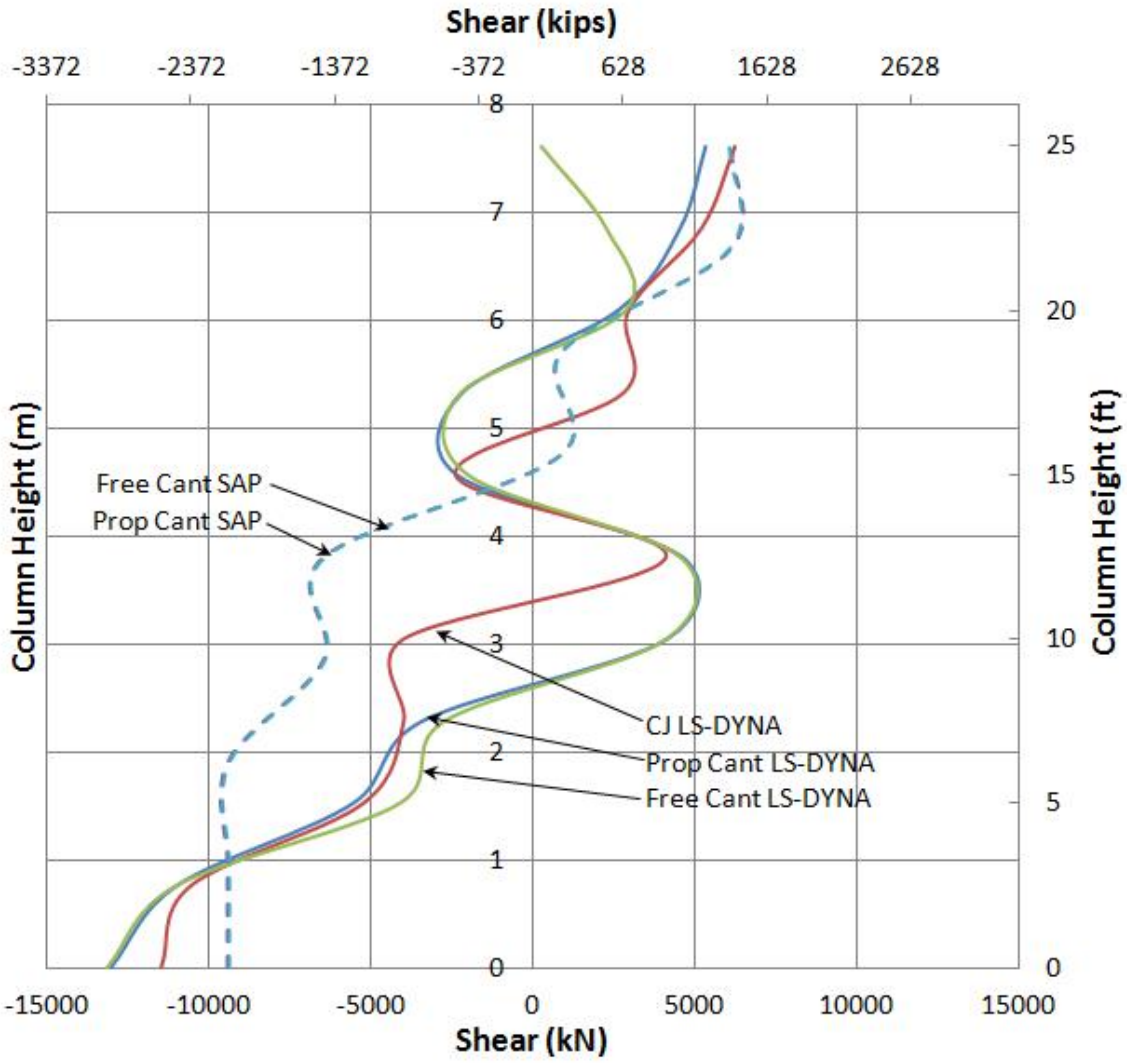

Figure 6-10 Shear Envelope, Group 3, L/d = 5, ρ = 2%, Z = 0.198 m/kg$^{1/3}$

6.4.3 Group 3 Deflected Shape

The deflected shape is shown in Figure 6-11 for Group 3 models. From Figure 6-11 it can be observed that the two SAP models have very similar deflected shapes except for the deflection at the top of the column in the free cantilever model. The deflection at the top of the column in the free cantilever LS-DYNA model is about twice as large as the deflection at the top of the free cantilever SAP model. The SAP models have approximately the same deflection at mid-height as the LS-DYNA models.

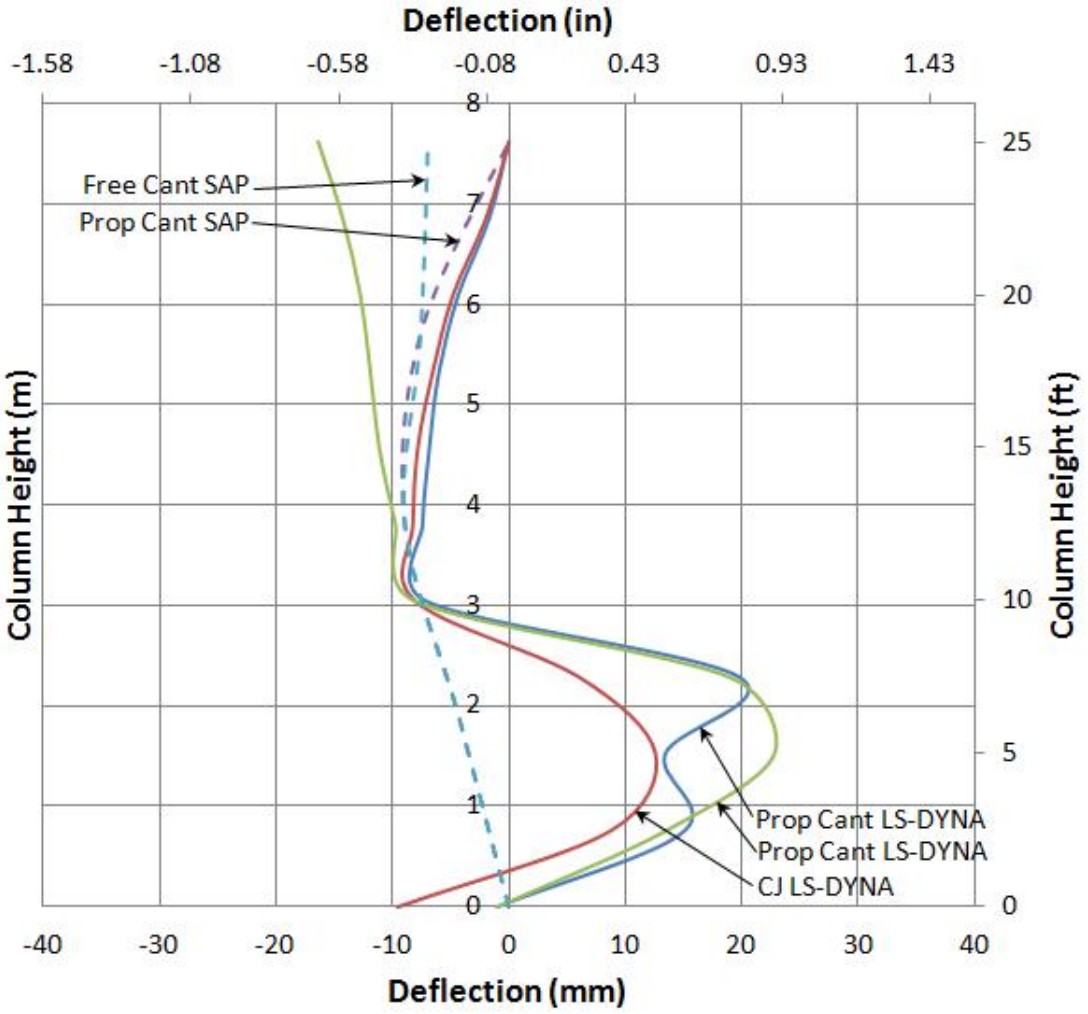

Figure 6-11 Deflected Shape, Group 3, L/d = 5, ρ = 2%, Z = 0.198 m/kg$^{1/3}$

6.5 Group 4 Results

Group 4 models have the following parameters: column aspect ratio, L/d, of 5; longitudinal reinforcement ratio, ρ, of 2%; and a scaled distance, Z, of 1.25 kg/m$^{1/3}$ (3.15 ft/lbm$^{1/3}$). The moment envelope, shear envelope, and deflected shape are presented for Group 4 models.

6.5.1 Group 4 Moment Envelope

The moment envelope for the Group 4 models is presented in Figure 6-12. It can be observed from Figure 6-12 that the moment envelopes of the two SAP models are very similar. The moment at the base of the column is approximately 3.5 times greater in the SAP models than in the propped cantilever and construction joint LS-DYNA models. The moment at the base of the column is approximately 2.25 times greater in the SAP models than in the free cantilever LS-DYNA model. The moments in the SAP models are about 2.25 times greater than the LS-DYNA models from approximately 3.0 m (9.8ft) from the base to the top of the column.

6.5.2 Group 4 Shear Envelope

The shear envelope for Group 4 models is presented in Figure 6-13. From Figure 6-13 it can be observed that the two SAP models have very similar shear envelopes. The free cantilever SAP model has the same shear at the top of the column as the propped cantilever SAP model due to the discrete mass of the superstructure modeled at the top of the column. The base shear in the SAP models is approximately two times greater than the LS-DYNA models. All three LS-DYNA models have approximately the same base shear. The SAP models and the propped cantilever and construction joint LS-DYNA models have approximately the same shear at the top of the column.

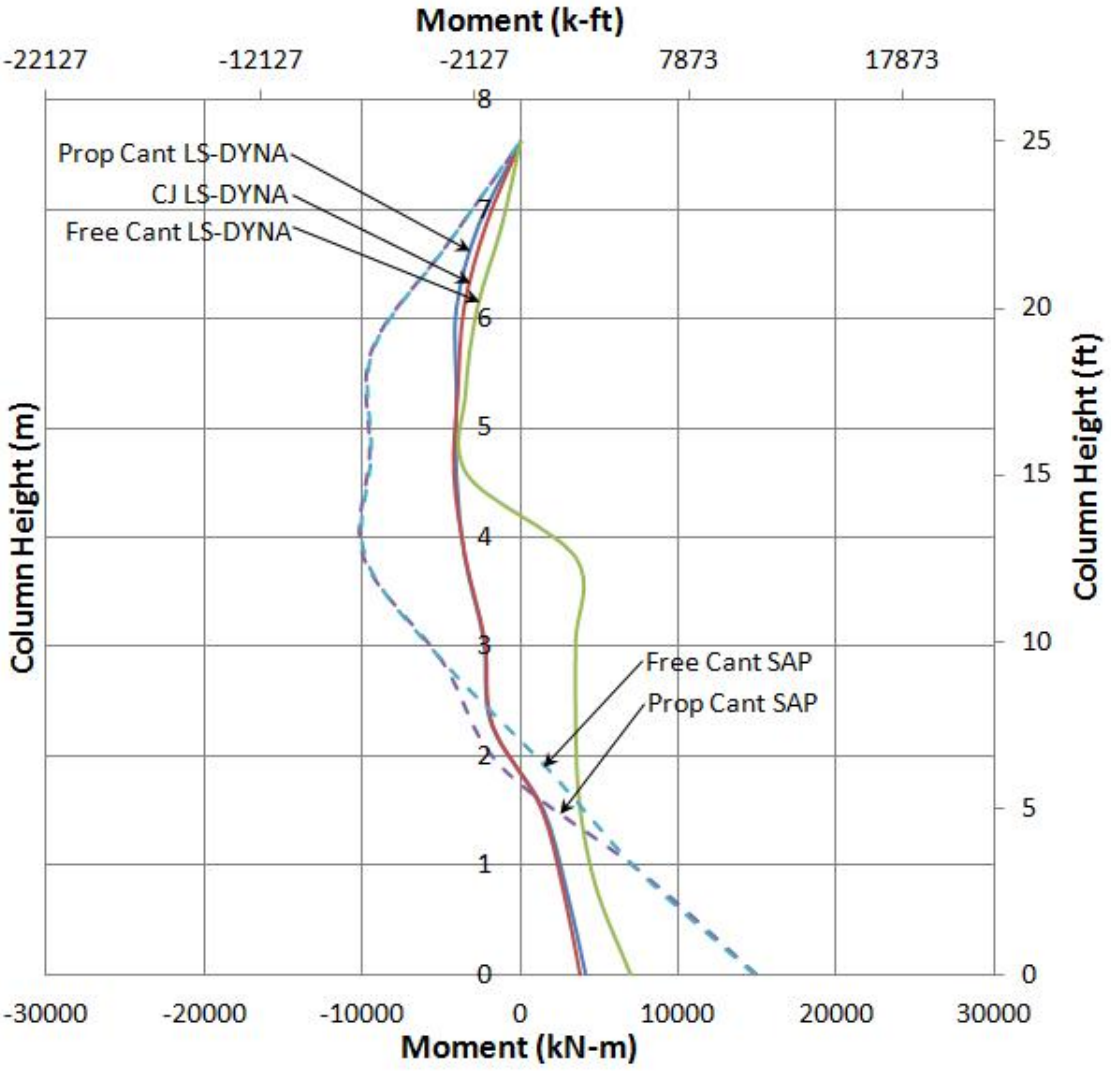

Figure 6-12 Moment Envelope, Group 4, L/d = 5, ρ = 2%, Z = 1.25 m/kg$^{1/3}$

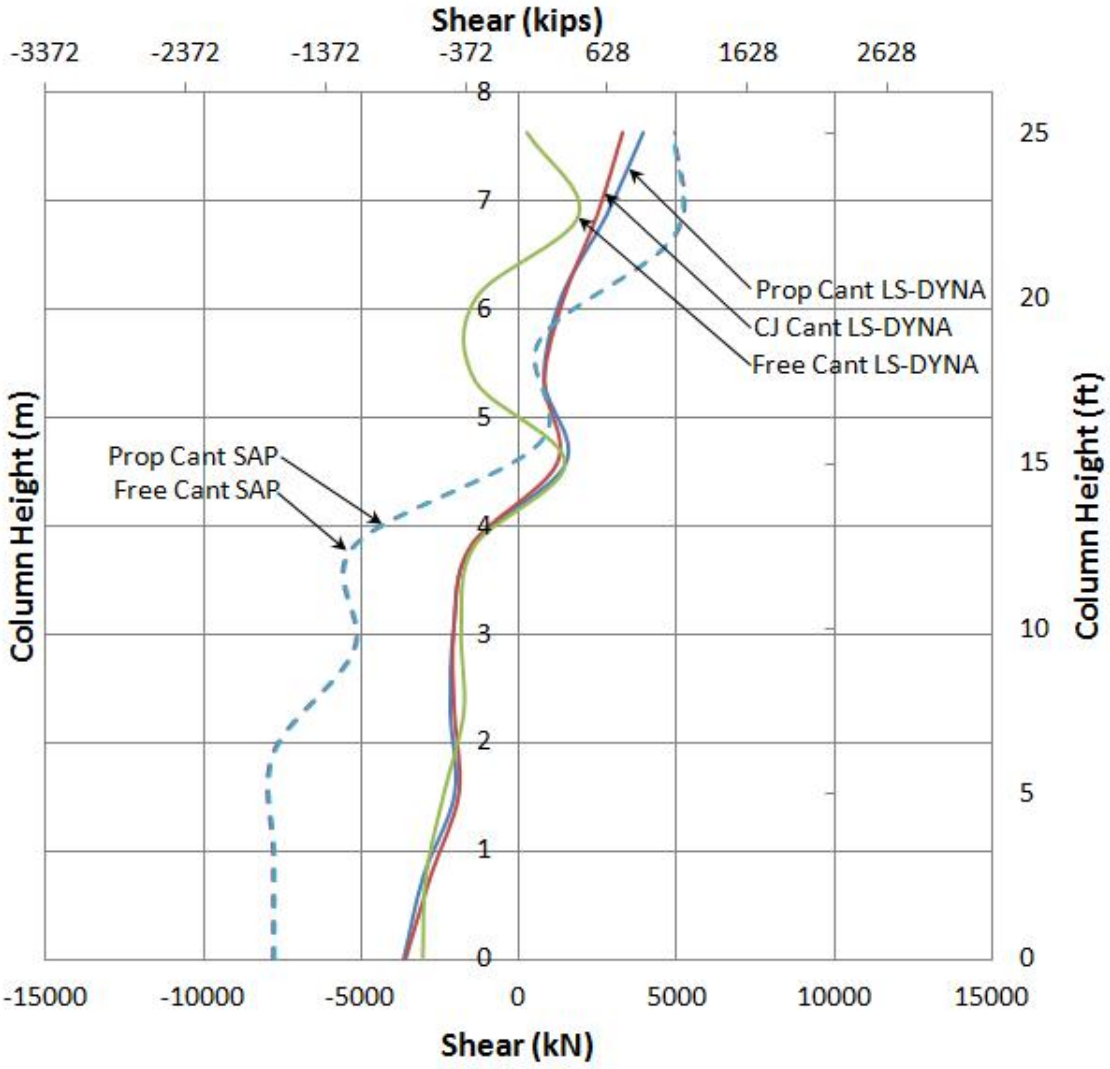

Figure 6-13 Shear Envelope, Group 4, L/d = 5, ρ = 2%, Z = 1.25 m/kg$^{1/3}$

6.5.3 Group 4 Deflected Shape

The deflected shape for Group 4 models is presented in Figure 6-14. From Figure 6-14 it can be observed that the two SAP models have very similar deflected shapes except for the deflection at the top of the column in the free cantilever model. The deflection at the top of the column in the free cantilever LS-DYNA model is approximately twice as big as the deflection at the top of the free cantilever SAP model.

The construction joint LS-DYNA model deflected shape is very similar to the propped cantilever LS-DYNA model. The deflection at mid-height in the SAP models is approximately 3 times larger than the propped cantilever and construction joint LS-DYNA models.

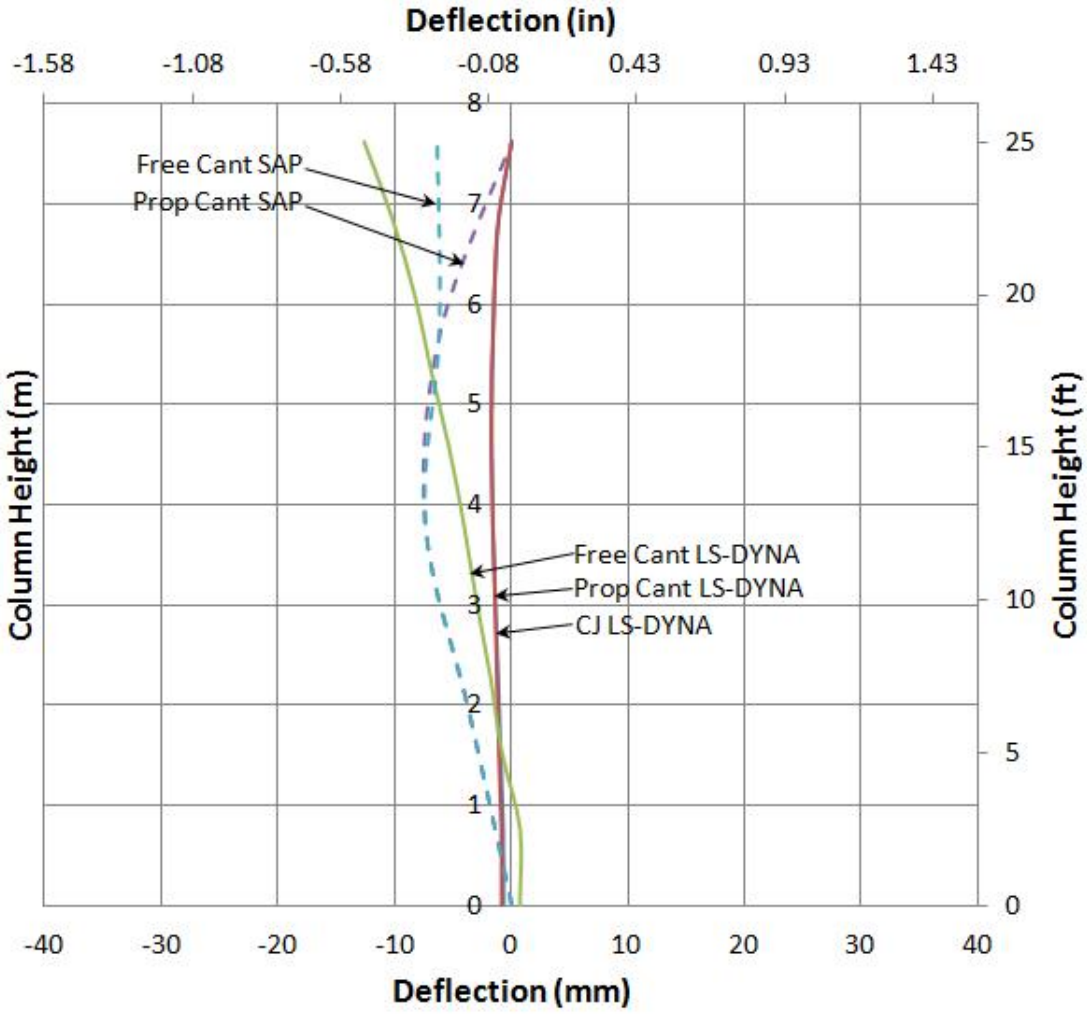

Figure 6-14 Deflected Shape, Group 4, L/d = 5, ρ = 2%, Z = 1.25 m/kg$^{1/3}$

6.6 Group 5 Results

Group 5 models have the following parameters: column aspect ratio, *L/d*, of 11; longitudinal reinforcement ratio, ρ, of 1%; and a scaled distance, *Z*, of 0.198 kg/m$^{1/3}$ (0.5 ft/lbm$^{1/3}$). The moment envelope, shear envelope, and deflected shape are presented for Group 5 models.

6.6.1 Group 5 Moment Envelope

The moment envelope for Group 5 models is presented in Figure 6-15. It can be observed from Figure 6-15 that the two SAP models have very similar moment envelopes. All three LS-DYNA models have approximately equal moments at the base of the column. The moment at the base of the column is approximately 3.5 times greater in the SAP models compared to the LS-DYNA models. The moments in the SAP models are about 3.33 times greater than the LS-DYNA models from approximately 8.0 m (26.25 ft) to 14.0 m (45.9 ft) from the base.

6.6.2 Group 5 Shear Envelope

The shear envelope for Group 5 models is presented in Figure 6-16. From Figure 6-16 it can be observed that the two SAP models have very similar shear envelopes. The base shear in all three LS-DYNA models is approximately the same. The shear at the base of the column is approximately two times greater in the LS-DYNA models than the SAP models. The shear at the top of the column is about 1.33 times greater in the SAP models compared to the propped cantilever and construction joint LS-DYNA models.

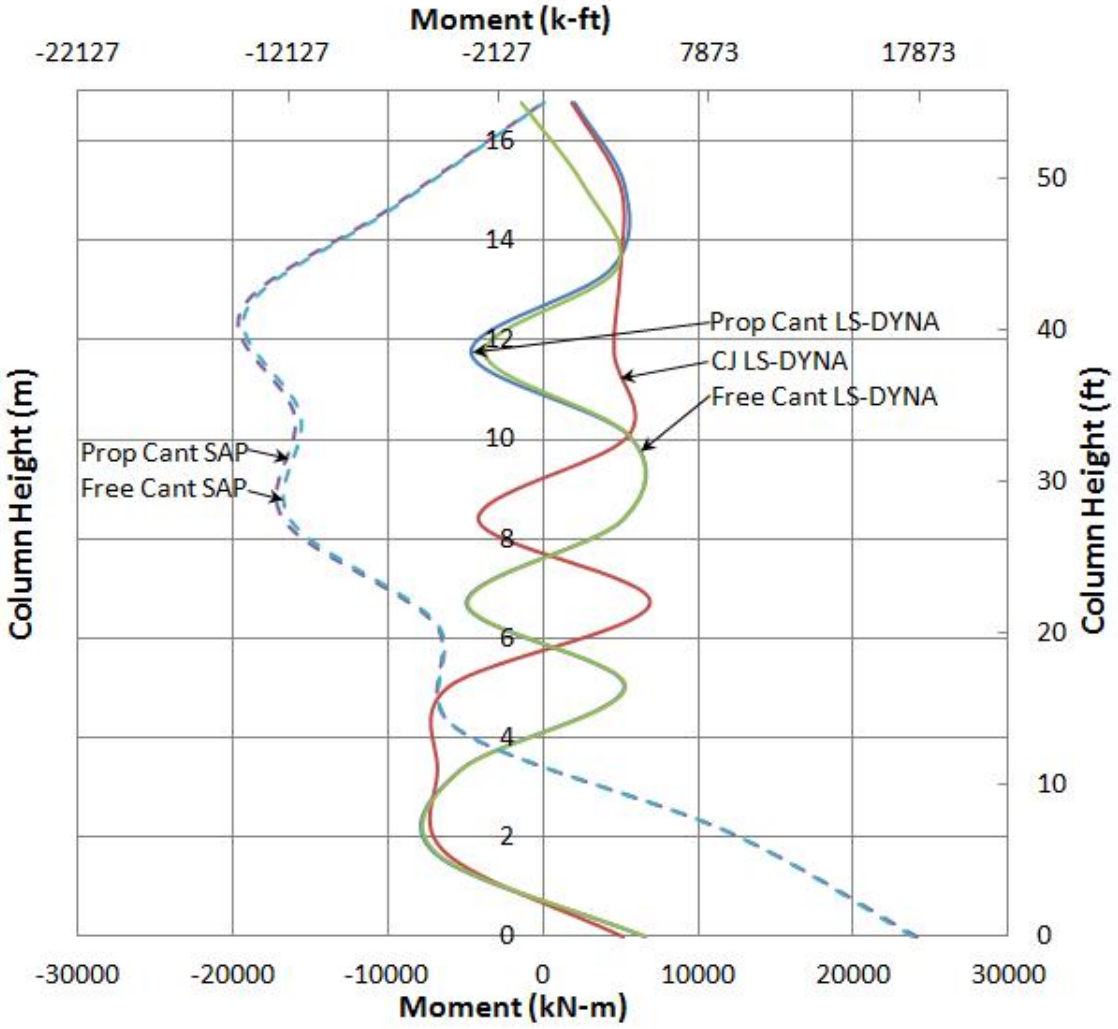

Figure 6-15 Moment Envelope, Group 5, L/d = 11, ρ = 1%, Z = 0.198 m/kg$^{1/3}$

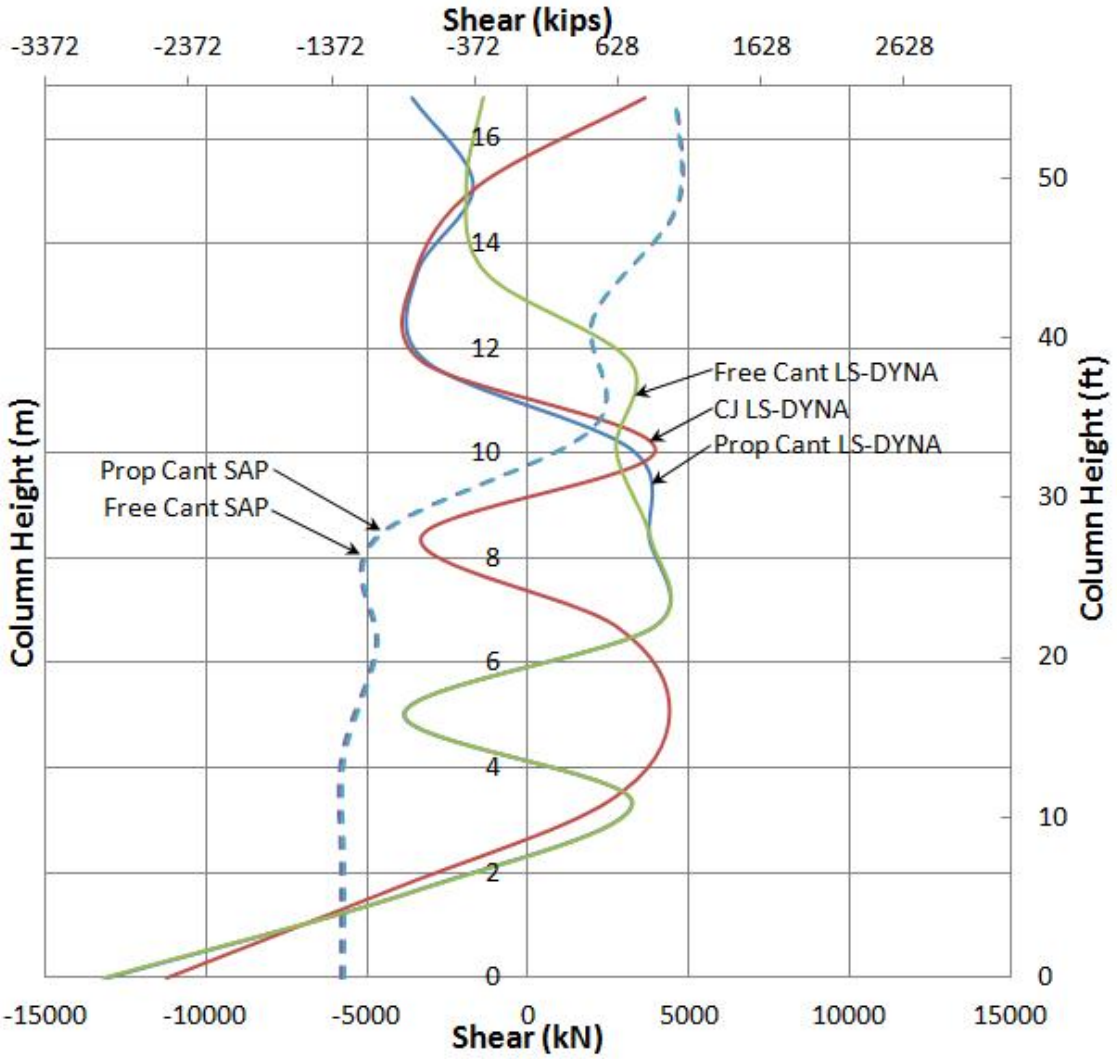

Figure 6-16 Shear Envelope, Group 5, L/d = 11, ρ = 1%, Z = 0.198 m/kg$^{1/3}$

6.6.3 Group 5 Deflected Shape

The deflected shape for Group 5 models is presented in Figure 6-17. From Figure 6-17 it can be observed that the two SAP models have approximately equal deflected shapes except for the deflection at the top of the column in the free cantilever model. The deflection at the top of the column in the free cantilever LS-DYNA model is approximately twice as large as the free cantilever SAP model. The deflection at mid-

height of the column in the SAP models is approximately 3.5 times larger than the LS-DYNA models.

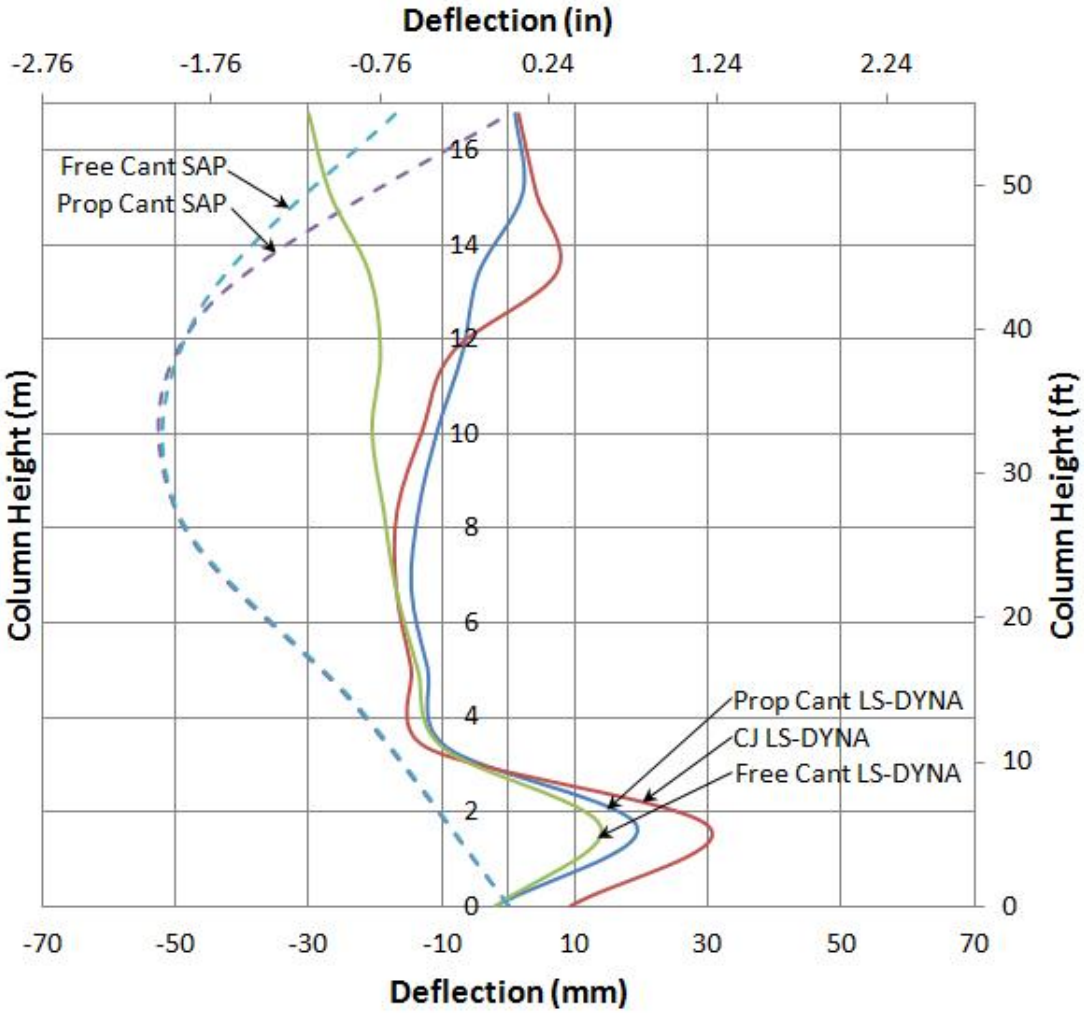

Figure 6-17 Deflected Shape, Group 5, L/d = 11, ρ = 1%, Z = 0.198 m/kg$^{1/3}$

6.7 Group 6 Results

Group 6 models have the following parameters: column aspect ratio, L/d, of 11; longitudinal reinforcement ratio, ρ, of 1%; and a scaled distance, Z, of 1.25 kg/m$^{1/3}$ (3.15

ft/lbm$^{1/3}$). The moment envelope, shear envelope, and deflected shape are presented for Group 6 models.

6.7.1 Group 6 Moment Envelope

The moment envelope for Group 6 models is presented in Figure 6-18. From Figure 6-18 it can be observed that the two SAP models have very similar moment envelopes. The three LS-DYNA models have approximately equal moments at the base of the column. The moment at the base of the column in the SAP models is approximately four times greater than in the LS-DYNA models. The moments in the SAP models is about 3.5 greater than the LS-DYNA models from approximately 8.0 m (26.25 ft) from the base to the top of the column.

6.7.2 Group 6 Shear Envelope

The shear envelope for Group 6 models is presented in Figure 6-19. It can be observed from Figure 6-19 that the two SAP models have approximately equal shear envelopes. All three LS-DYNA models have approximately the same base shear. The base shear in the SAP models is approximately two times greater than the base shear in the LS-DYNA models. The shear at the top of the column is approximately two times greater in the SAP models compared to the LS-DYNA models.

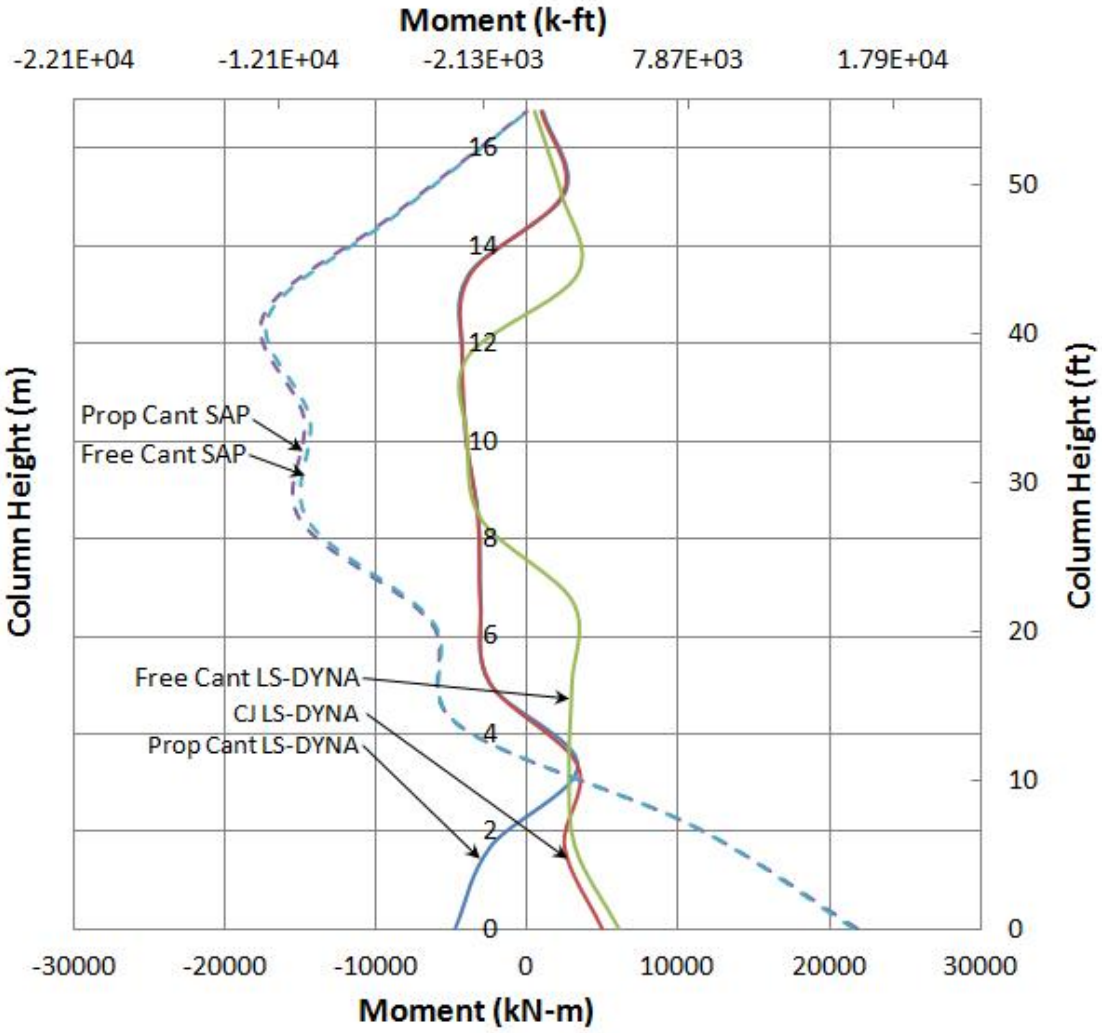

Figure 6-18 Moment Envelope, Group 6, L/d = 11, ρ = 1%, Z = 1.25 m/kg$^{1/3}$

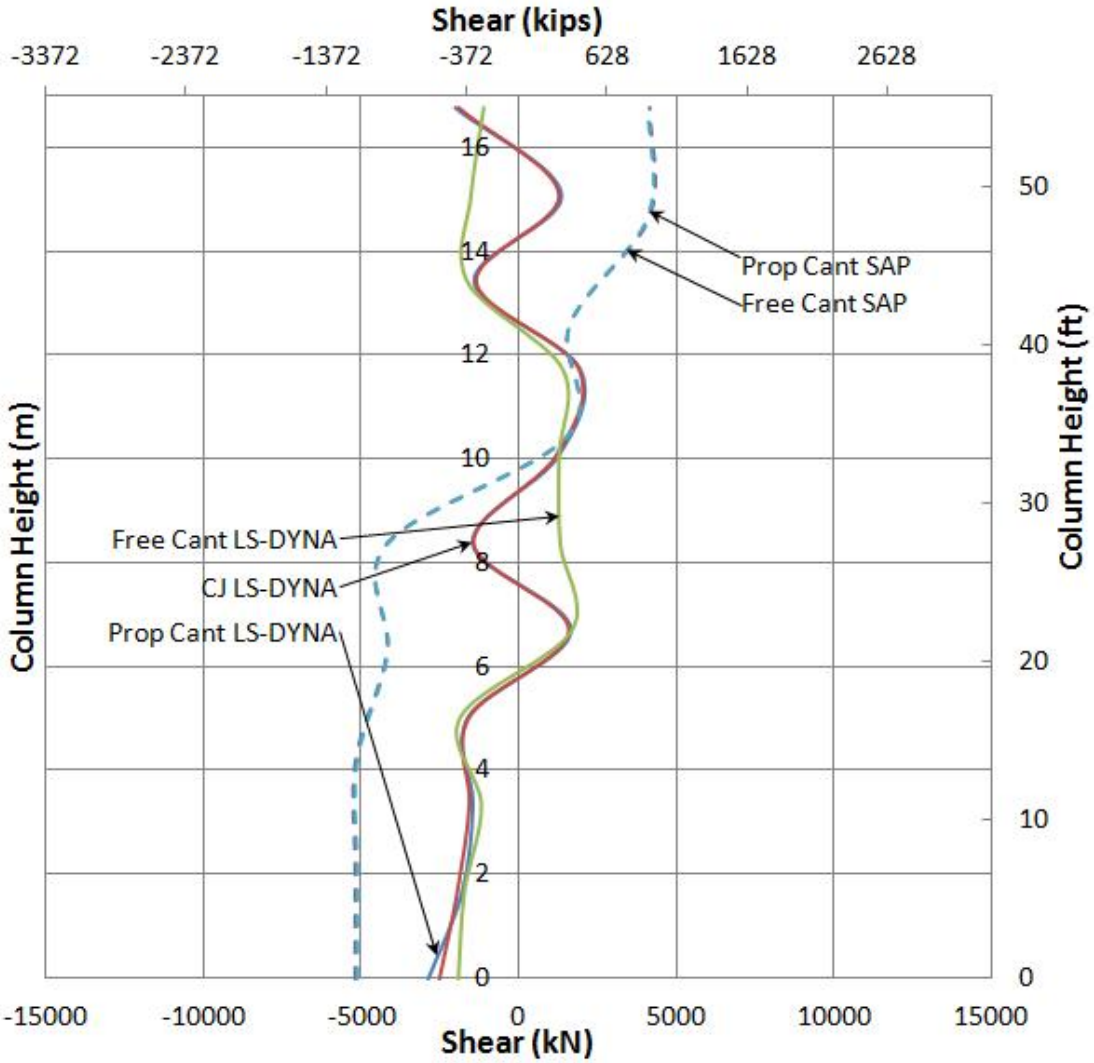

Figure 6-19 Shear Envelope, Group 6 L/d = 11, ρ = 1%, Z = 1.25 m/kg$^{1/3}$

6.7.3 Group 6 Deflected Shape

The deflected shape for Group 6 models is presented in Figure 6-20. From Figure 6-20 it can be observed that the two SAP models have very similar deflected shapes except for the deflection at the top of the column in the free cantilever model. The propped cantilever and construction joint LS-DYNA models have very similar deflected

shapes. The deflection at mid-height in the SAP models is approximately 5 times greater than the propped and construction joint LS-DYNA models.

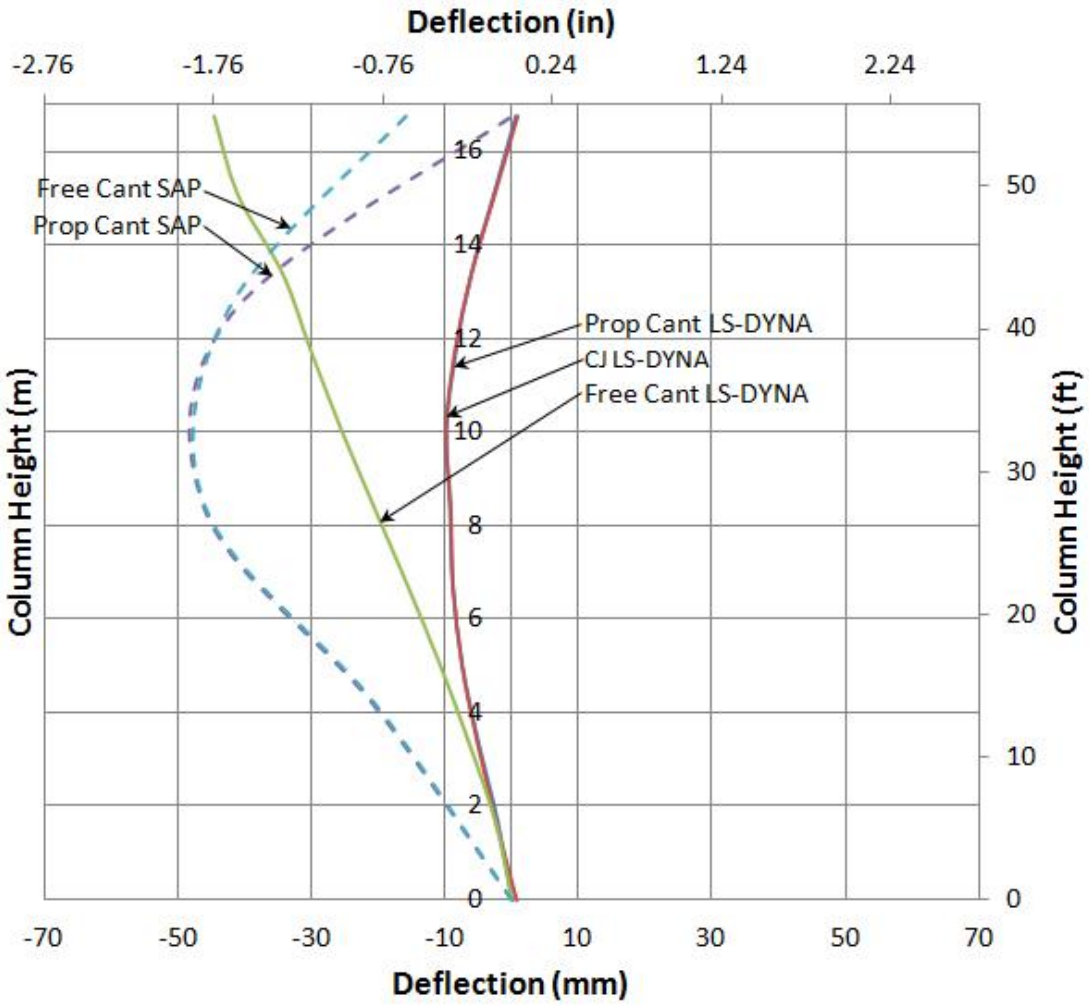

Figure 6-20 Deflected Shape, Group 6 L/d = 11, ρ = 1%, Z = 1.25 m/kg$^{1/3}$

6.8 Group 7 Results

Group 7 models have the following parameters: column aspect ratio, L/d, of 11; longitudinal reinforcement ratio, ρ, of 2%; and a scaled distance, Z, of 0.198 kg/m$^{1/3}$ (0.5 ft/lbm$^{1/3}$). The moment envelope, shear envelope, and deflected shape are presented for Group 7 models.

6.8.1 Group 7 Moment Envelope

The moment envelope for Group 7 models is presented in Figure 6-21. From Figure 6-21 it can be observed that the moments at the base of the column are approximately equal in all three LS-DYNA models. The moments at the base of the column in the SAP models are approximately four times greater than the LS-DYNA models. The moments in the SAP models are about 2.5 times greater than the LS-DYNA models from approximately 8.0 mm (26.25 ft) from the base to the top of the column.

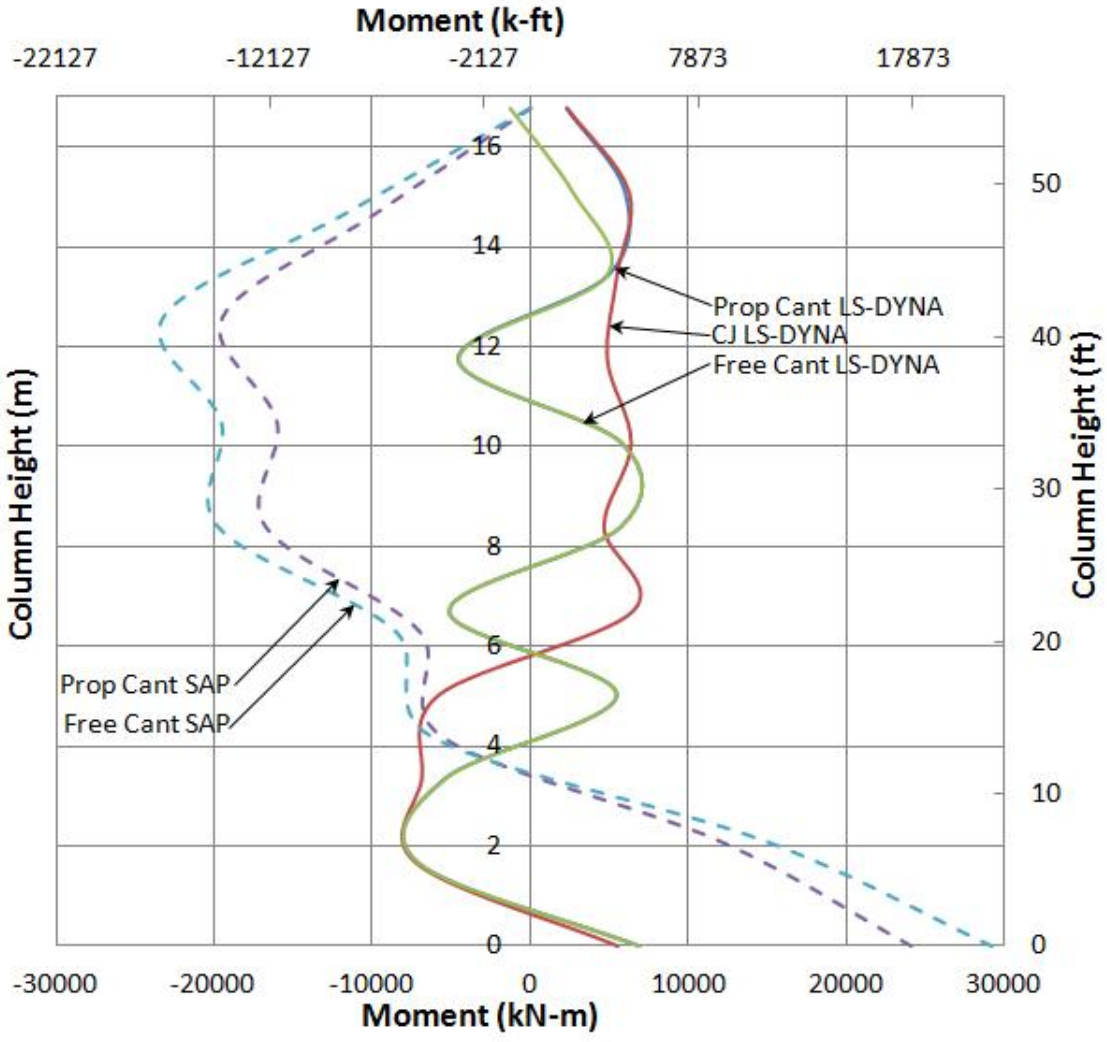

Figure 6-21 Moment Envelope, Group 7, L/d = 11, ρ = 2%, Z = 0.198 m/kg$^{1/3}$

6.8.2 Group 7 Shear Envelope

The shear envelope for Group 7 models is presented in Figure 6-22. It can be observed from Figure 6-22 that the shear at the base of the column in all three LS-DYNA models is approximately equal. The shear at the base of the column in the LS-DYNA models is approximately two times greater than the SAP models. The shear in the SAP models is about equal to the shear in the LS-DYNA models from approximately 6.0 m (19.7 ft) from the base to the top of the column.

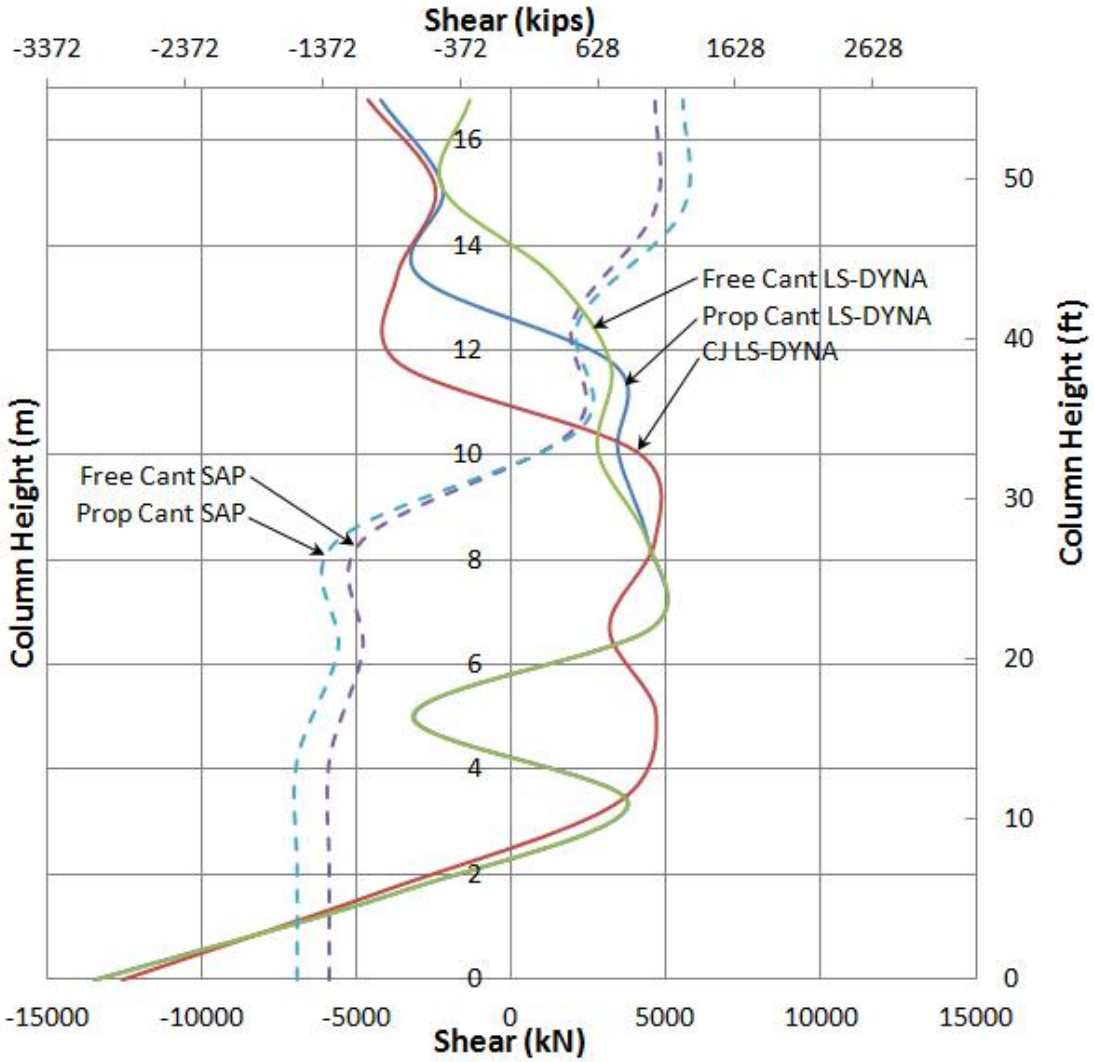

Figure 6-22 Shear Envelope, Group 7, L/d = 11, ρ = 2%, Z = 0.198 m/kg$^{1/3}$

6.8.3 Group 7 Deflected Shape

The deflected shape for Group 7 models is presented in Figure 6-23. From Figure 6-23 it can be observed that the two SAP models have very similar deflected shapes except for the deflection at the top of the column in the free cantilever model. The deflection of the free cantilever SAP model is approximately 1.2 times greater than the propped cantilever SAP model. The deflection at mid-height of the column in the free cantilever SAP model is approximately 6.33 times greater than the propped cantilever and construction joint LS-DYNA models.

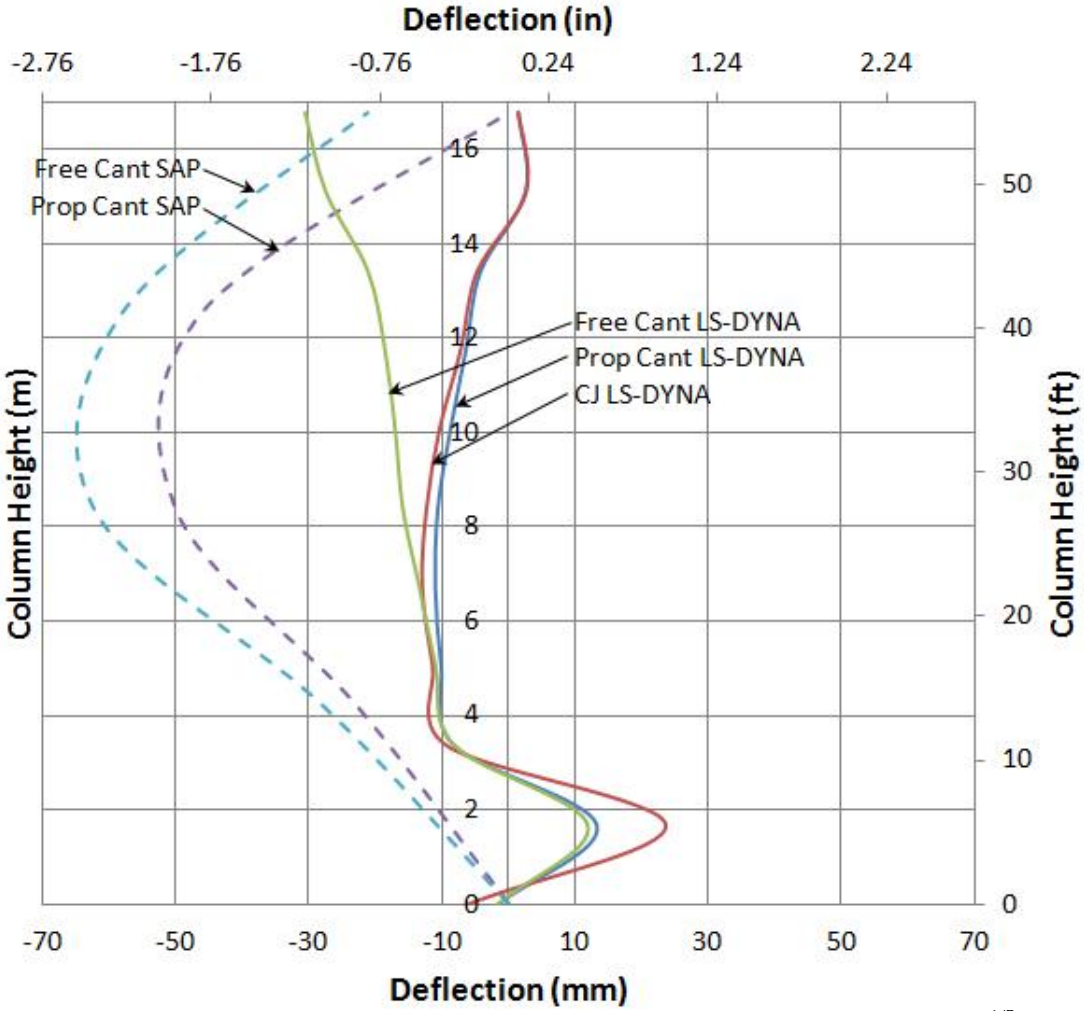

Figure 6-23 Deflected Shape, Group 7, L/d = 11, ρ = 2%, Z = 0.198 m/kg$^{1/3}$

6.9 Group 8 Results

Group 8 models have the following parameters: column aspect ratio, *L/d,* of 11; longitudinal reinforcement ratio, ρ, of 2%; and a scaled distance, *Z*, of 1.25 kg/m$^{1/3}$ (3.15 ft/lbm$^{1/3}$). The moment envelope, shear envelope, and deflected shape are presented for Group 8 models.

6.9.1 Group 8 Moment Envelope

The moment envelope for Group 8 models is presented in Figure 6-24. From Figure 6-24 it can be observed that the moment at the base of the column is approximately equal for all three LS-DYNA models. The moment at the base of the column in the propped cantilever SAP model is approximately 2.25 times greater than the LS-DYNA models. The moment at the base of the column in the free cantilever SAP model is approximately four times greater than the LS-DYNA models. The moment in the propped cantilever SAP model is about two times greater than the LS-DYNA models from approximately 8.0 m (26.25 ft) from the base to the top of the column. The moment in the free cantilever SAP model is about 3.5 times greater than the LS-DYNA models from approximately 8.0 m (26.25 ft) from the base to the top of the column.

6.9.2 Group 8 Shear Envelope

The shear envelope for Group 8 models is presented in Figure 6-25. It can be observed from Figure 6-25 that the base shear in all three LS-DYNA models is approximately equal. The base shear in the propped cantilever SAP model is approximately 1.33 times greater than the LS-DYNA models. The base shear in the free

cantilever SAP model is approximately 2.25 times greater than the LS-DYNA models. The shear at the top of the column in the propped cantilever SAP model is approximately equal to the LS-DYNA models. The shear at the top of the column in the free cantilever SAP model is about 1.75 times greater than the LS-DYNA models.

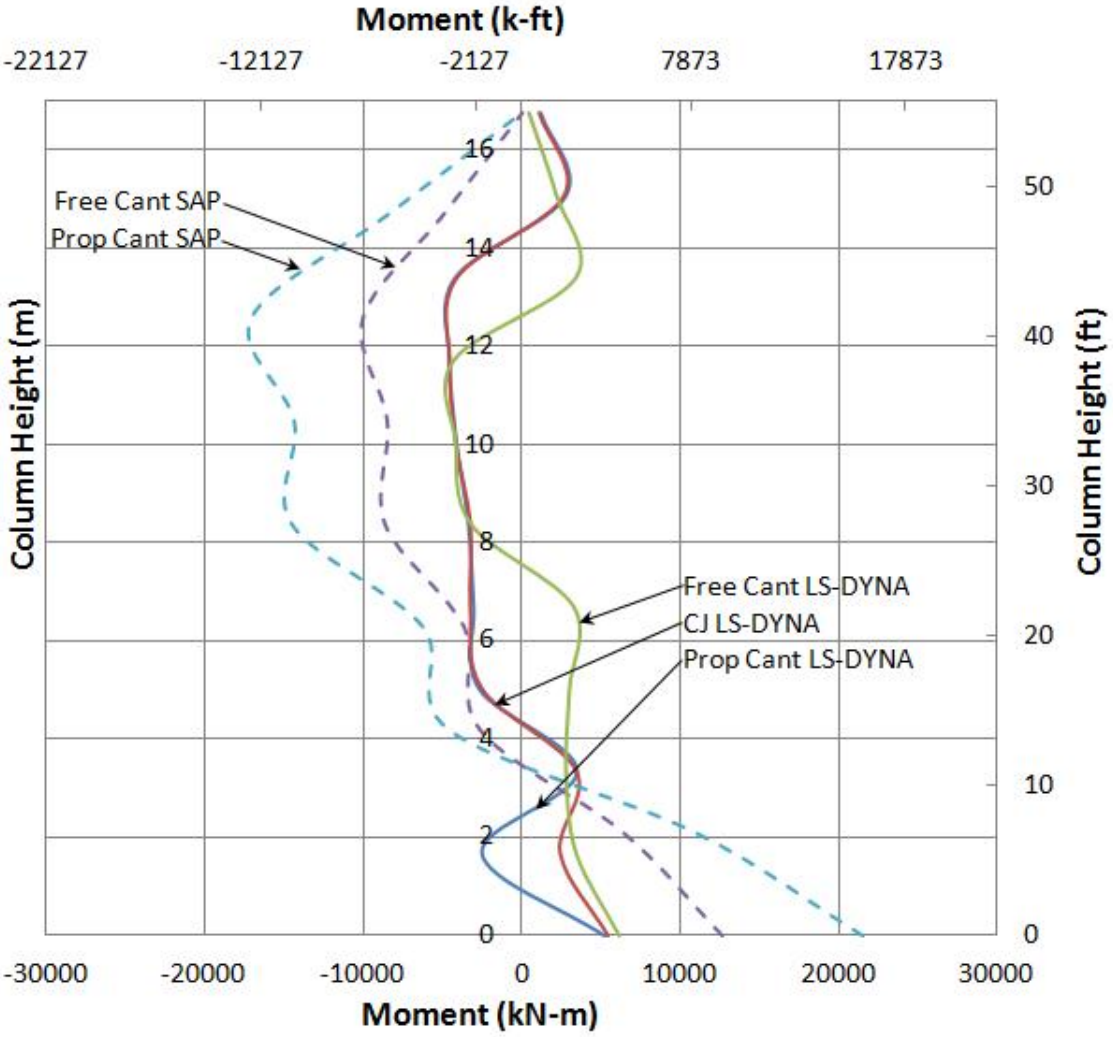

Figure 6-24 Moment Envelope, Group 8, L/d = 11, ρ = 2%, Z = 1.25 m/kg$^{1/3}$

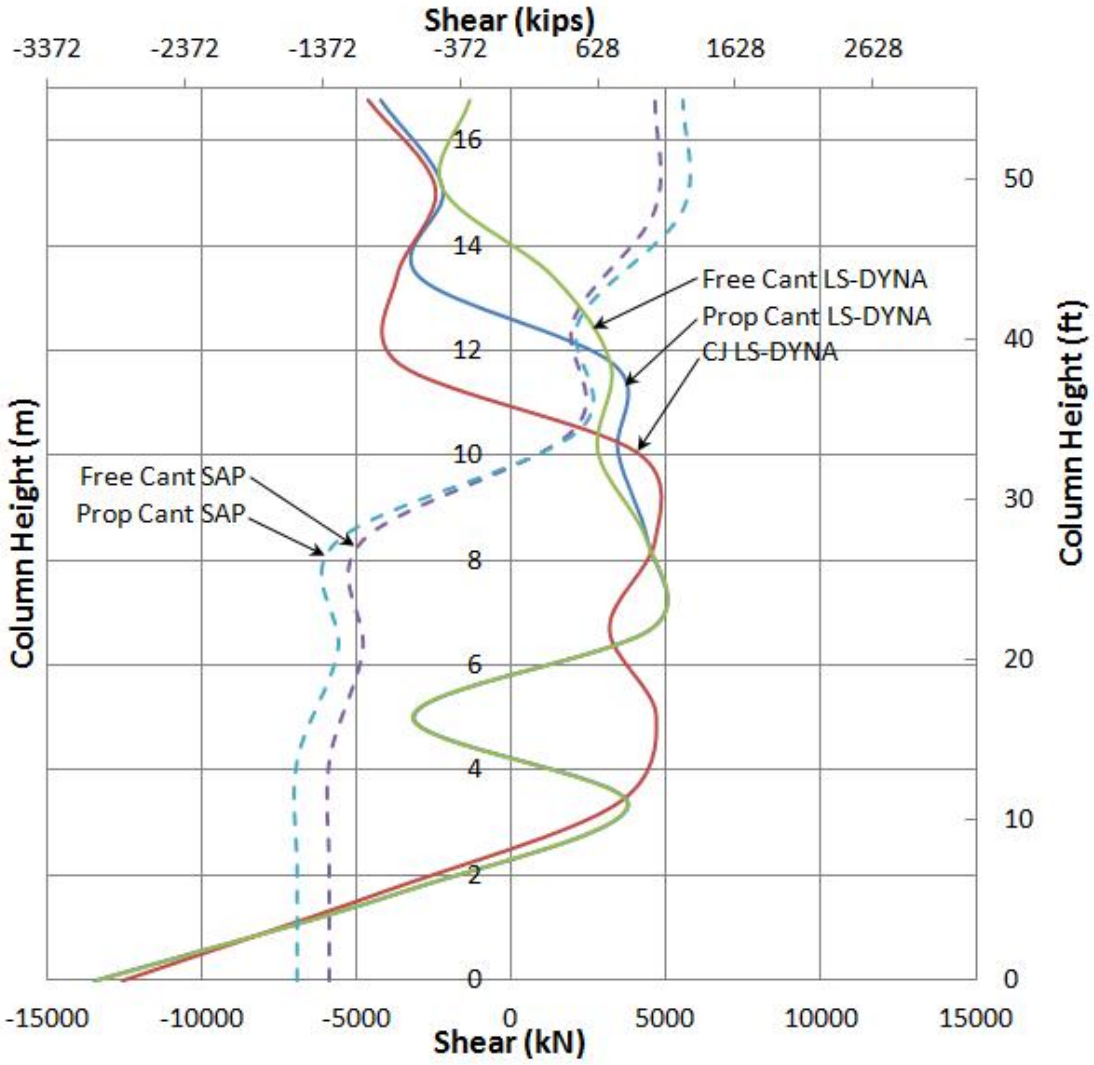

Figure 6-25 Shear Envelope, Group 8, L/d = 11, ρ = 2%, Z = 1.25 m/kg$^{1/3}$

6.9.3 Group 8 Deflected Shape

The deflected shape for Group 8 models is presented in Figure 6-26. From Figure 6-26 it can be observed that the free cantilever SAP model has deflections that are approximately 1.67 times greater than the propped cantilever SAP model. The maximum deflection of the free cantilever SAP model is approximately 5 times larger than the propped and construction joint LS-DYNA models.

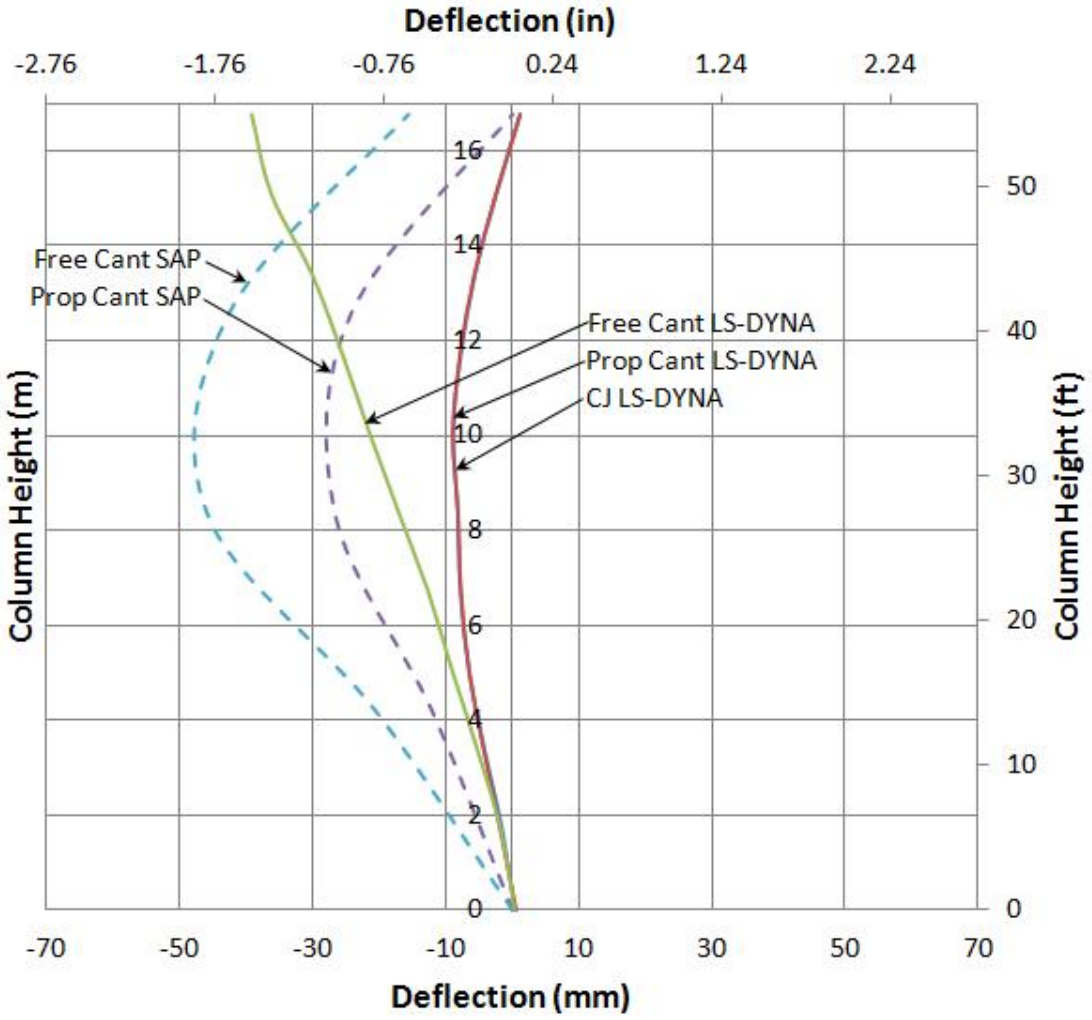

Figure 6-26 Deflected Shape, Group 8, L/d = 11, ρ = 2%, Z = 1.25 m/kg$^{1/3}$

6.10 Deflection-Time History

The deflection-time histories for Groups 3, 4, 7, and 8 are presented in Figures 6-27 through 6-30. The deflection-time histories of the free cantilever SAP and LS-DYNA models are not shown for clarity. Similarly, groups with ρ = 1% are not graphed because of their similarity in behavior to their corresponding ρ = 2% models. These four graphs illustrate the deflection – time history of the propped cantilever SAP and LS-DYNA

models of the short and tall columns subject to the two different blast scaled distances. . The graphs correspond to the deflected shape of 0.75*H, where H = the height of the column. These graphs will be evaluated to investigate the frequency and corresponding period of the SAP and LS-DYNA models. The SAP models were moved from t = 0 to approximately t = 0.01 seconds to align with the initial deflections recorded in the LS-DYNA models.

The SAP and LS-DYNA models have very similar frequencies throughout all four graphs. In the short column models, the SAP models have periods that are slightly larger than the corresponding LS-DYNA models. The largest difference in frequency is in the short column with the small blast load. In this case, the SAP model has period of approximately 0.024 seconds and the LS-DYNA model has a period of approximately 0.020 seconds. Tall column models in SAP and LS-DYNA have very similar periods subject to both the small and large blast load. Considering a comparison between the LS-DYNA models, the construction joint model always has a slightly larger period than the propped cantilever model. This trend is true for all four graphs.

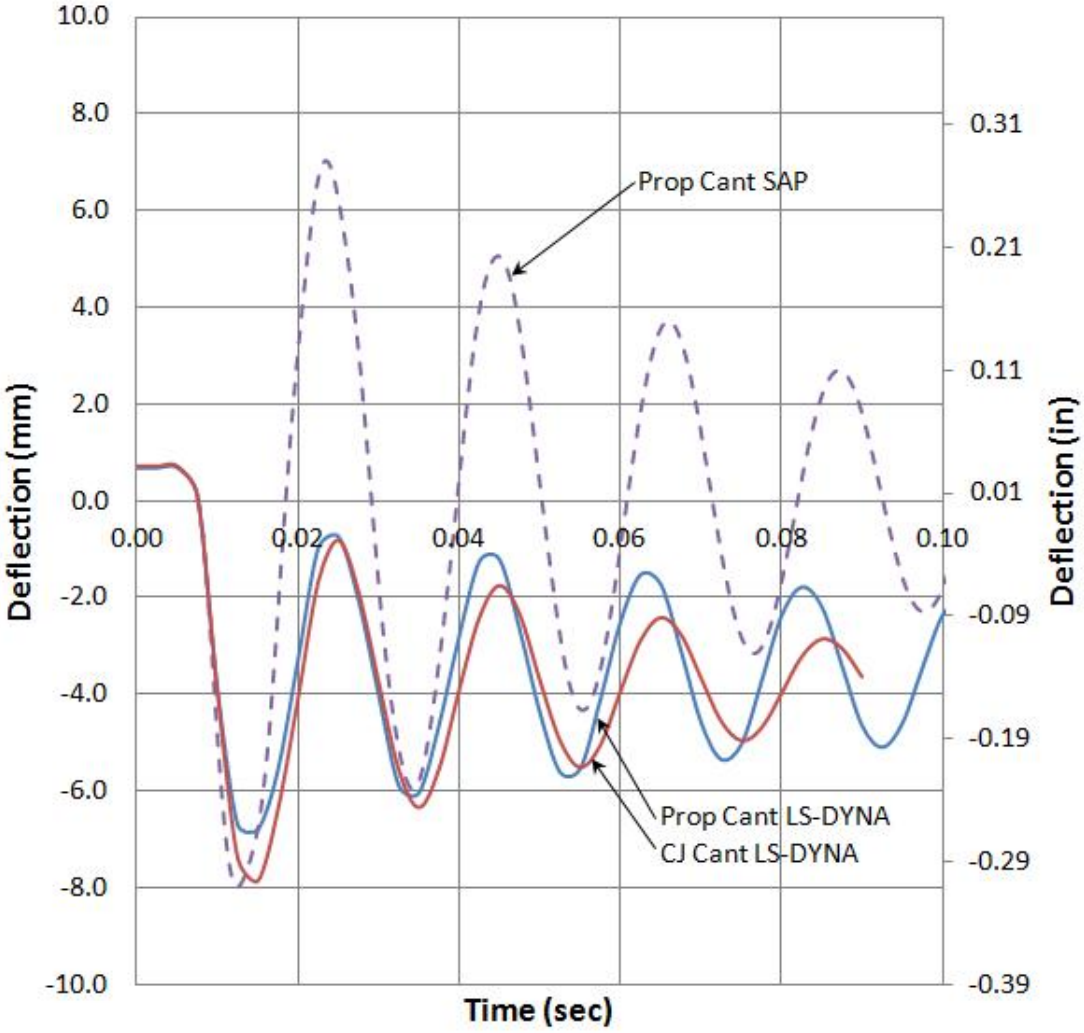

Figure 6-27 Deflection-Time History, Group 3, L/d = 5, ρ = 2%, Z = 0.198 m/kg$^{1/3}$

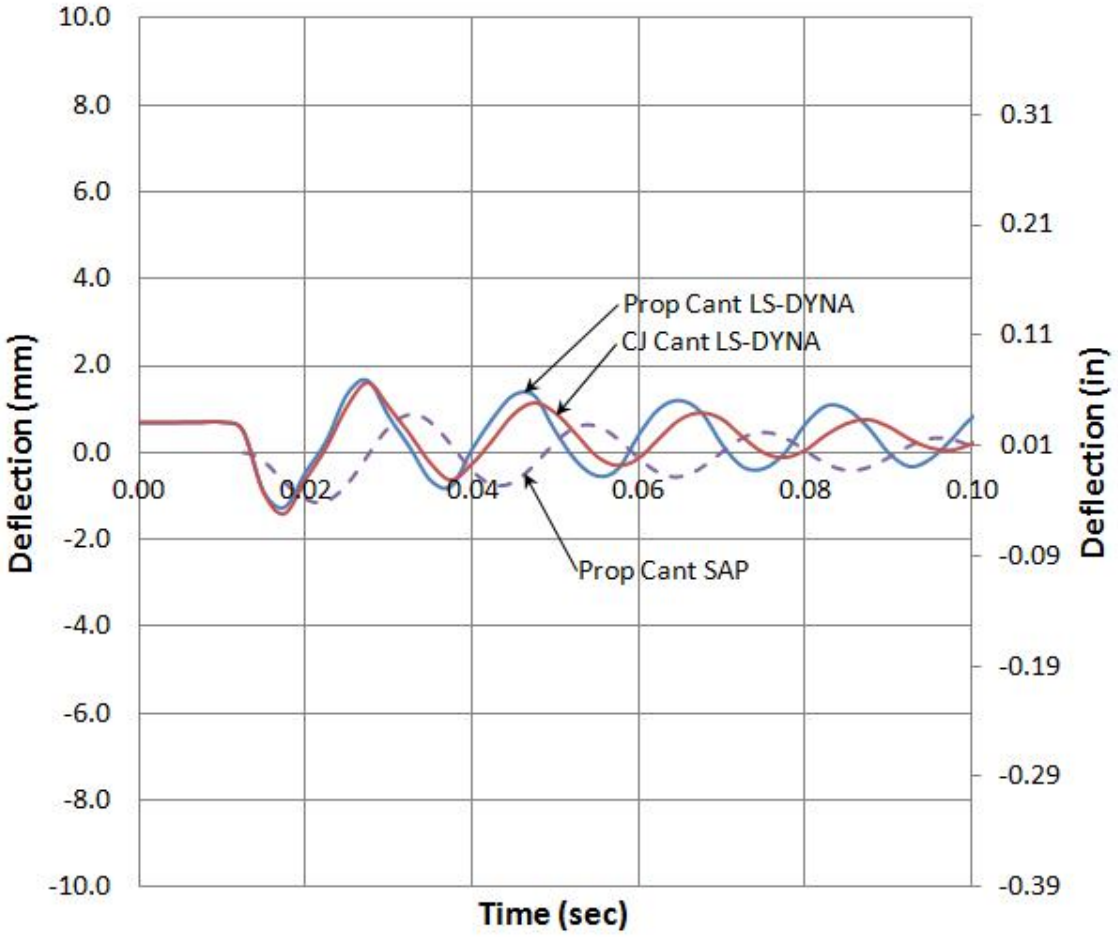

Figure 6-28 Deflection-Time History, Group 4, L/d = 5, ρ = 2%, Z = 1.25 m/kg$^{1/3}$

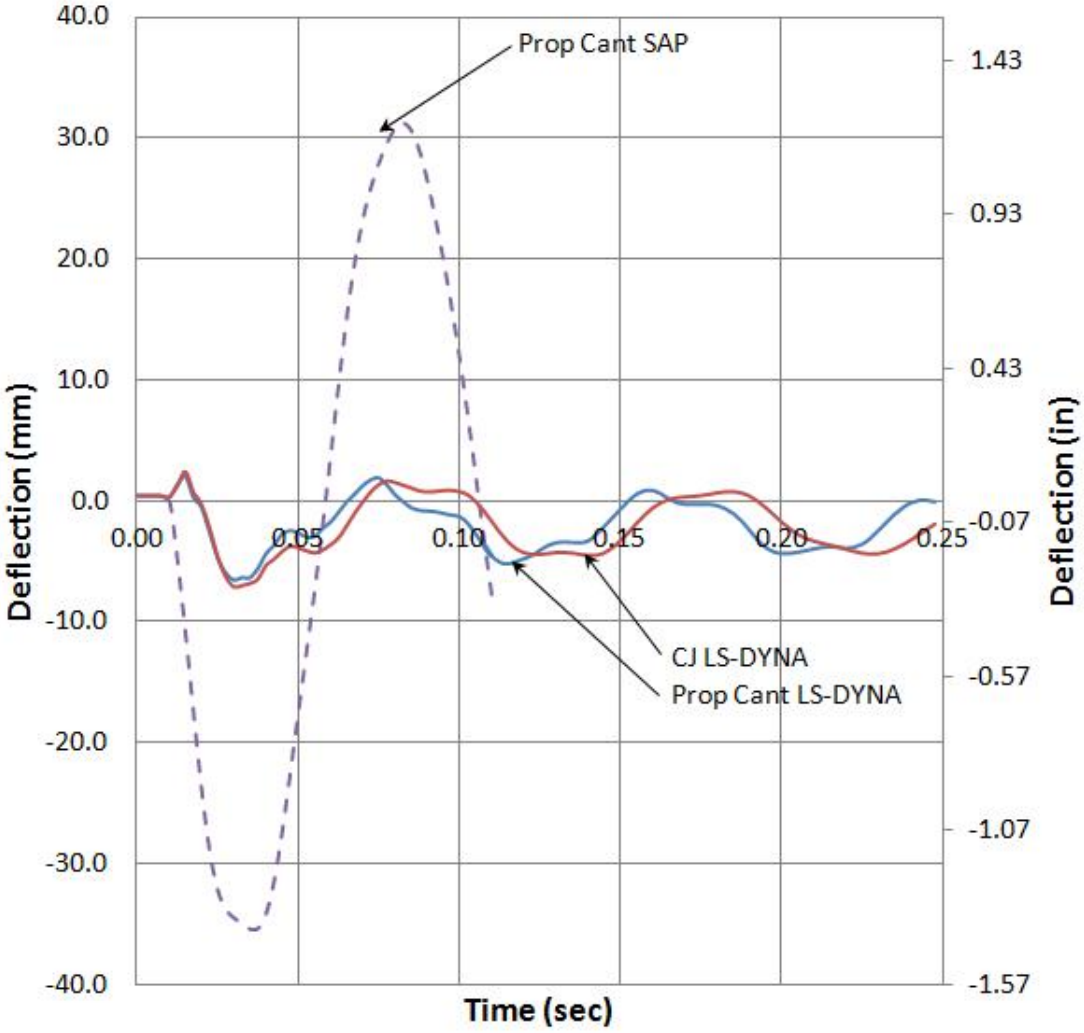

Figure 6-29 Deflection-Time History, Group 7, L/d = 11, ρ = 2%, Z = 0.198 m/kg$^{1/3}$

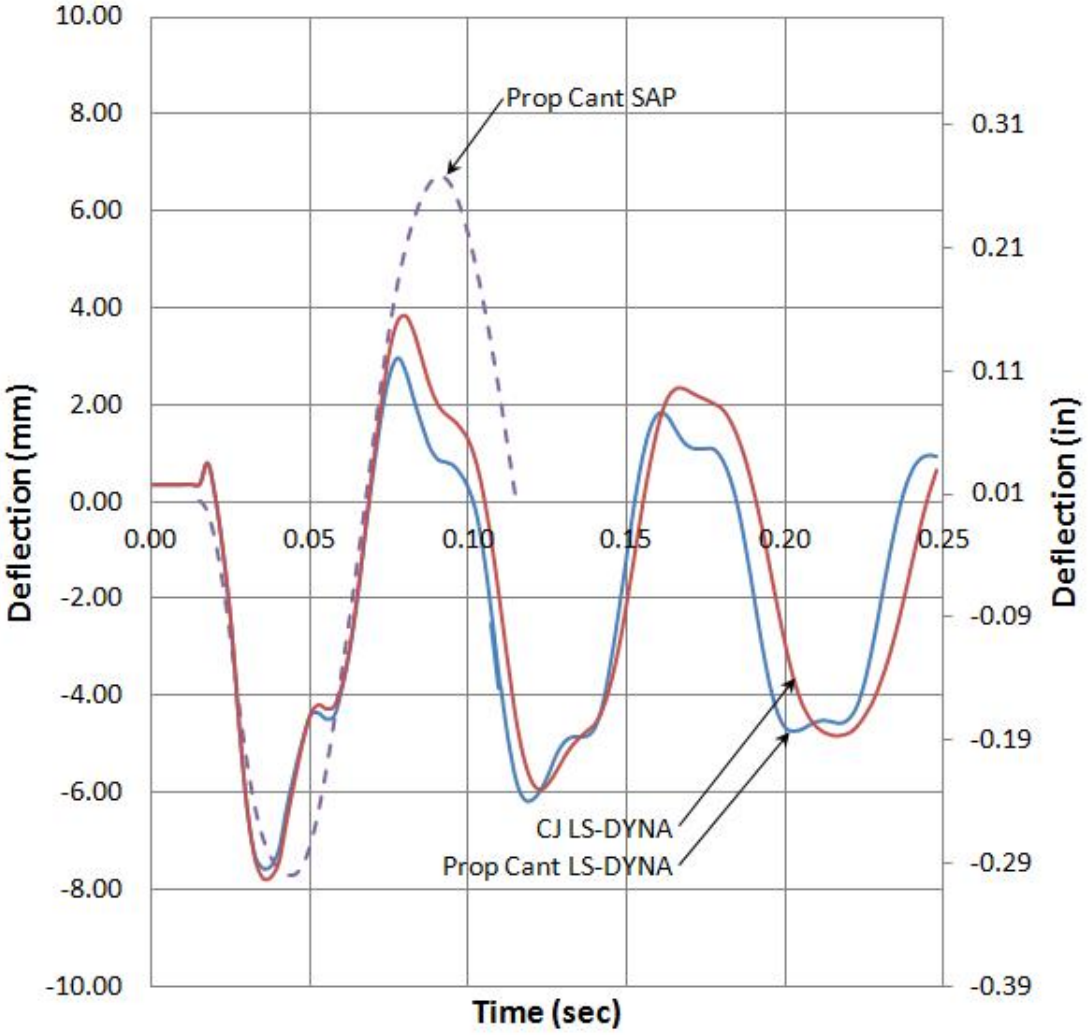

Figure 6-30 Deflection-Time History, Group 8, L/d = 11, ρ = 2%, Z = 1.25 m/kg$^{1/3}$

6.11 Discussion

Eight groups of models were graphed to illustrate moment, shear, and deflected shape performance. Models were grouped together with similar parameters of aspect ratio, longitudinal reinforcement ratio, and scaled distances. The LS-DYNA models were assumed to be the baseline for the evaluation of the SAP models. Global comparisons

between groups with respect to moment, shear, and deflection behavior are discussed below.

The SAP models in all groups have higher moments at the base and mid-height of the column compared to the moments in the LS-DYNA models. There is a greater difference in moments between the LS-DYNA and SAP models in groups with an aspect ratio of 11 compared to groups with an aspect ratio of 5.

With $Z = 0.198$ kg/m$^{1/3}$ (0.5 ft/lbm$^{1/3}$), the SAP models have lower base shear than the LS-DYNA models. However, with $Z = 1.25$ kg/m$^{1/3}$ (3.15 ft/lbm$^{1/3}$), the LS-DYNA models have lower base shear than the SAP models. The shear at the top of the column is the same in the propped cantilever and free cantilever SAP models due to the discrete mass of the superstructure modeled at the top of the column. The base shear in the LS-DYNA models is approximately equal in models with $L/d = 5$ and $L/d = 11$ at each scaled distance. However, the SAP models have lower base shear with $L/d = 11$ compared to $L/d = 5$ at each scaled distance. LS-DYNA models indicate that base shear should not be impacted by aspect ratio but only blast load. Base shear in the SAP models with $L/d = 5$ is greater than the models with $L/d = 11$.

The SAP models have greater deflections at mid-height of the column compared to the LS-DYNA models. Aspect ratio has a more significant impact on deflection than scaled distance. The difference in deflection between the LS-DYNA and SAP models is greater with a scaled distance of 1.25 m/kg$^{1/3}$ than with a scaled distance of 0.198 m/kg$^{1/3}$.

Load effects are generally overestimated in the SAP models compared to the LS-DYNA models due to several modeling parameters. These parameters include load application, material behavior, and mass distribution.

The load application differs between the SAP and LS-DYNA models because the LS-DYNA models are a coupled analysis where as the SAP models are an uncoupled analysis. Therefore, material yield and structure response do not affect the applied loads in the SAP models. The load effects in the SAP models are overestimated because the reduced stiffness of the column after yielding and failure is not taken into account. The loads in the LS-DYNA models are coupled with the structure response giving more accurate load application throughout the blast event.

The load application differences in SAP and LS-DYNA include the initial load magnitude, arrival time, and distribution. The blast load is applied to the SAP model at peak incident pressure at $t = 0$, as shown in Figures 6-1 and 6-2. This pressure linearly decreases to zero over a time equal to the duration of the CONWEP loading used in the LS-DYNA load application. The LS-DYNA models have an initial pressure loading of zero at $t = 0$, as shown in Figures 6-1 and 6-2. This load increases to the maximum incident pressure and then has a non-linear decrease in pressure. Therefore the SAP models do not undergo the first part of the loading event, which increases from zero to the maximum load. This is significant because the performance and capacity of the SAP models cannot be evaluated at loads below the peak incident pressure. Therefore, it cannot be determined if the capacity of the column is reached before the peak incident pressure is applied. It is recommended that the SAP models include the arrival time so that they are subjected to the increase of the applied blast load, such that the initial load equals zero at $t = 0$ and is increased to maximum incident pressure similar to the CONWEP load application. Using this load application, it could be determined if the ultimate capacity of the column is reached before the maximum load is applied.

In addition, the blast load is applied uniformly along the height of the SAP models but varies along the height of the LS-DYNA models. The maximum incident pressure from CONWEP was applied along the height of the column at each discrete mass in the SAP models. In the LS-DYNA models, load application to the column was determined using computational fluid dynamics. Therefore, the pressure applied along the height of the LS-DYNA models vary in magnitude and in arrival time.

Material behavior is another significant difference between the SAP and LS-DYNA models. The SAP models are composed of elements defined by linear behavior, while the LS-DYNA models include plastic behavior response. Linear behavior does not accurately capture the ultimate capacity, deformation or energy absorption of the column. The SAP models report moments and shears greater than the column's capacity because they exhibit constant stiffness beyond yield. In addition, the SAP models do not incorporate a cracked section modulus or stiffness reduction for yielded or failed elements. In highly dynamic problems, energy absorption is an important consideration of design. Structural elements are designed for plastification to dissipate energy and allow for safe ductile failures of critical components. Linear material models cannot be used for determining plastic material response, plastic deformations, or energy absorption behavior. If linear material models are used, it is recommended that cracked or damaged sections be modeled with reduced stiffness.

It is thought that the differences in base shear behavior between the SAP and LS-DYNA models is dependent on the load application, particularly that the SAP models are subject to distributed load along the full-height of the column and the LS-DYNA models are applied a pressure which varies in magnitude and arrival-time along the height of the

column. Williamson et al. (2010) found that pressures at the top of the column are lower and arrive much later than at the bottom of the column and suggest that superstructure elements need not be modeled because pressure confined by these components will not control column response. Similarly, it can be found in the present study's LS-DYNA models that load application is concentrated in the bottom third of the column height. Because the majority of models include a boundary condition at the top of the column (or concentrated lumped mass that provides a large resisting inertia force), the column behaves similarly to a beam with fixed and pin end supports.

The resultant force acting on the SAP models is close to mid-height, and therefore, the base shear in the SAP models are not as sensitive to the increased blast load pressure. For example in Figures 6-7 (low blast load) and 6-4 (high blast load) – the base shear increases from approximately 8 kN to 9.5 kN. In the LS-DYNA models, the resultant blast load is much closer to the base of the column and is much more sensitive to blast load magnitude. An example of these results can be seen in Figures 6-7 (low blast load) and 6-4 (high blast load) – the base shear increases from approximately 2 kN to 12,000 kN. Therefore, it is believed that the location of the resultant load application, along with arrival time and the coupled analysis is the reasoning for the reverse base shear trends in the SAP and LS-DYNA models with respect to scaled distance.

From Figures 6-27 through 6-30, it can be determined that the SAP and LS-DYNA model frequencies are consistent. Column height and blast load magnitude do not cause any particular discrepancies in the results with respect to model frequency behavior. Therefore, it can be determined that the mass distribution in the SAP models,

which uses four discrete masses is a sufficient modeling approximation as compared the LS-DYNA models which use a uniform mass distribution.

Chapter 7

Summary, Conclusions, and Recommendations

7.1 Summary and Conclusions

The objectives of this study were to evaluate a simplified modeling technique of a bridge column subjected to blast loads by comparing results to a validated finite element model. The performance of these models was evaluated by comparing moment, shear, and deformation magnitudes over the time-history of a blast event.

The following conclusions can be drawn from the evaluation of the results:

1. The longitudinal reinforcement ratio has little to no effect on moment or shear behavior in LS-DYNA models and SAP models in Groups 1 through 6.
2. The longitudinal reinforcement ratio has little to no effect on the deformation behavior of the SAP models and the propped cantilever and construction joint LS-DYNA models.
3. The most significant contributor to the behavior differences in the simplified model compared to the LS-DYNA model is difference in stiffness between the two models. The LS-DYNA model includes cracking and plastic behavior, whereas the SAP model has linear elastic behavior.
4. The lumped mass of the superstructure at the top of the SAP models causes the free cantilever to behave like a propped cantilever. This can be

explicitly observed in the shear results for the free cantilever SAP models. The shear force present at the top of the column is a result of the inertia effects of the lumped mass in the free cantilever models. The free and propped cantilever models have similar moment, shear, and deformation behavior throughout all groups.

5. The SAP and LS-DYNA models have similar frequencies. Therefore, the discretization of the mass in the SAP models is a sufficient modeling approximation.

7.2 Recommendations

It is recommended to use a finite element model for the analysis of bridge columns subjected to blast loads. The parameters used in this study dictated no clear trends between the LS-DYNA models and the simplified models.

If a simplified analysis is required, the following recommendations are made:

1. The stiffness of the linear elements should be reduced to better represent a cracked section. The stiffness of the elements could be determined by checking the ultimate capacity of the column.
2. The mass of the superstructure at the top of the column significantly influences the behavior of the free cantilever. For the case of a free cantilever, it is recommended to apply an axial load equal to the weight of the superstructure to the column instead of adding the mass of the superstructure to the top mass.

3. It is recommended that the loads in the SAP models be scaled down from the pressures calculated with CONWEP such that their effects match LS-DYNA models despite not being able to account for yielding and failure. The loads could be scaled by checking the ultimate capacity of the column to better represent plastic behavior of the column.
4. The boundary condition at the top of the column should be accurately modeled to represent the bearing condition present.

7.3 Future Research

7.3.1 Element Stiffness

Cracking, crushing, and spalling of concrete has a significant impact on column response to blast loads. Further investigation of how to determine the reduced stiffness of the linear elements in the simplified model is needed.

7.3.2 Loads

The loads applied in the simplified model need to be further investigated. The loads should be scaled down to better represent the behavior of the column after yielding has occurred. The scaling of the loads could be determined by testing the ultimate capacity of the column.

7.3.3 Boundary Conditions

The boundary condition at the top of the column in both the LS-DYNA and simplified models need to be investigated. Springs could be used to better model the stiffness of the superstructure and bearing configuration. The number of girders,

continuity at the pier, skew of the bridge, bearing pad conditions, and other bridge configuration parameters could be taken into account with springs.

7.3.4 Modeling Parameters

Mesh density and mass distribution in simplified models need to be further researched. This study only considered four elements and four lumped masses along the height of the column. The LS-DYNA models defined the mass of the column much more realistically. The SAP and LS-DYNA models in this study have similar frequencies, which indicates a sufficient approximation in the SAP models. However, more research needs to be done to determine the appropriate number of discrete masses in the simplified models for other column configurations.

7.3.5 Reinforcement

Consideration of reinforcement in this study was very limited. Transverse reinforcement was constant and only two ratios were considered for longitudinal reinforcement. Increasing the amount of transverse reinforcement improves the column's response to blast loads by increasing ductility and confinement (NCHRP Report 645). Modeling techniques should be developed that capture the influence of reinforcement detailing.

References

American Association of State Highway and Transportation Officials. (2013). *AASHTO LRFD Bridge Design Specifications,* 6th Edition. Washington, D.C.

Baylot, J.T., Ray, J.C. and Hall, R.L. (2003). "Prediction Method for Response of Steel Bridge Beams and Girders to Blast and Fragment Loads." *Transportation Research Record*. 69-74.

Computers & Structures, Inc. (2013). *CSI Analysis Reference Manual For SAP2000, ETABS, and SAFE*. CSI, Berkeley.

Fujikura, S., Bruneau, M. (2008). "Experimental and Analytical Investigation of Blast Performance of Seismically Resistant Bridge Piers." Technical Report MCEER-08-0028.

FHWA. (2003). "Recommendations for Bridge and Tunnel Security." Federal Highway Administration, prepared by the Blue Ribbon Panel on Bridge and Tunnel Security, Washington, D.C.

FHWA. (2011). "Evaluation of LS-DYNA Concrete Material Model 159." Federal Highway Administration, Washington, D.C.

Hopkinson, B. (1915). British Ordnance Board Minutes, 13565.

Islam, A.K.M.A., and Yazdani, N. (2008). "Performance of AASHTO Girder Bridges under Blast Loading." *Engineering Structures*, 30 (2008), 1922-1937.

LSTC. (2014). *LS-DYNA Theory Manual*. Livermore Software Technology Company, Livermore.

LSTC. (2014). *LS-DYNA Keyword User Manual, Version 971*. Livermore Software Technology Corporation, Livermore.

Magallanes, J.M. (2008). "Importance of Concrete Material Characterization and Modeling to Predicting the Response of Structures to Shock and Impact Loading." *Structures Under Shock and Impact X*. WIT Press: Southampton, UK. 241-50.

Malvar, L.J., Crawford, J., Wesevich, J., and Simons, D. (1997). "A Plasticity Concrete Material Model for DYNA3D." *Int. J. Impact Engng.*, 19(9-10), 847-873.

Malvar, L.J. (1998). "Review of Static and Dynamic Properties of Steel Reinforcing Bars." *ACI Materials Journal*, 9(5), 609-616.

Montgomery, D. (2009). *Design and Analysis of Experiments*. Hoboken: John Wiley & Sons, Inc.

Ngo, T., Mendis, P., Gupta A., and Ramsay, J. (2007). "Blast Loading and Blast Effects on Structures—An Overview." *ESJE Special Issue: Loading on Structures*, 76-91.

O'Hare, E. (2011). *Computational Assessment of Steel-Jacketed Bridge Pier Column Performance Under Blast Loads*. M.S. thesis, Pennsylvania State Univ., University Park, PA.

Priestley, M.J.N., Seible, F., Xiao, Y., and Verma, R. (1994). "Steel Jacket Retrofitting of Reinforced Concrete Bridge Columns for Enhanced Shear Strength - Part 1: Theoretical Considerations and Test Design." *ACI Structural Journal*, 91(4), 394-405.

Randers-Pehrson, G., and Bannister, K.A. (1997). *Airblast Loading Model for DYNA2D and DYNA3D*. Army Research Laboratory.

Science Applications International Corporation (SAIC). (1994). *International Blast and Thermal Environment for Internal and External Explosions: A User's Guide for the BLASTX Code.* Version 3.0. (SAIC 405-94-2)

Sriram, R., Vaidya, U.K., and Kim, J.-E. (2006). "Blast Impact Response of Aluminum Foam Sandwich Composites." *Springer Science and Business Media Inc.*, 4023-39.

Department of the Army. (1990). *Structures to Resist the Effects of Accidental Explosions (TM 5-1300).* Washington, D.C.

Departments of the Army, Air Force, and Navy and the Defense Special Weapons Agency. (2002). *Design and Analysis of Hardened Structures to Conventional Weapons Effects. United Facilities Criteria (UFC) 3-340-01.* Washington, D.C.

Departments of the Army, Air Force, and Navy and the Defense Special Weapons Agency. (2008). *Structures to Resist the Effects of Accidental Explosions. United Facilities Criteria (UFC) 3-340-02.* Washington, D.C.

Williamson, E.B. et al. (2010). *Blast Resistant Highway Bridges: Design and Detailing Guidelines*. Washington, D.C. NCHRP Report 645.

Winget, D.G., Marchland, K.A., and Williamson, E.B. (2005). "Analysis and Design of Critical Bridges Subjected to Blast Loads." *ASCE Journal of Structural Engineering*, 131(8), 1243-1255.